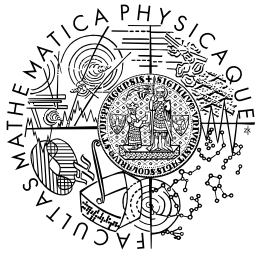

FACULTY
OF MATHEMATICS
AND PHYSICS
Charles University

MASTER THESIS

Lukáš Polcar

Geodesic chaos in a perturbed Schwarzschild field

Institute of Theoretical Physics

Supervisor of the master thesis:	doc. RNDr. Oldřich Semerák DSc.
Study programme:	Physics
Study branch:	Theoretical Physics

Prague 2018

I declare that I carried out this master thesis independently, and only with the cited sources, literature and other professional sources.

I understand that my work relates to the rights and obligations under the Act No. 121/2000 Sb., the Copyright Act, as amended, in particular the fact that the Charles University has the right to conclude a license agreement on the use of this work as a school work pursuant to Section 60 subsection 1 of the Copyright Act.

In ..... date ..... signature of the author

I would like to thank my supervisor Oldřich Semerák for the patient guidance, encouragement and advice he has provided throughout my time as his student. I also appreciate the numerous consultations with Petra Suková, Georgios Lukes-Gerakopoulos and Ondřej Kopáček at the Astronomical institute. And lastly I would like to thank to my family for their sustained support during my studies.

Název práce: Geodetický chaos v porušeném Schwarzschildově poli

Autor: Lukáš Polcar

Ústav: Ústav teoretické fyziky

Vedoucí diplomové práce: doc. RNDr. Oldřich Semerák DSc., Ústav teoretické fyziky

Abstrakt: Tato práce se zabývá studiem geodetického pohybu ve statickém, axiálně symetrickém prostoročase tvořeném superpozicí černé díry s diskem či prstencem. Tento systém budeme studovat pomocí dvou analytických metod, které nevyžadují řešení pohybových rovnic. První metodou je takzvané geometrické kritérium chaosu, které je založené na výpočtu vlastních čísel Riemannova tenzoru. Druhým přístupem pak je Melnikovova metoda, jež je schopna detekovat chaos ve slabě porušeném systému obsahujícím homoklinickou orbitu. Výsledky obou metod budou následně testovány numericky.

Klíčová slova: obecná teorie relativity, geodetická deviace, chaos v černoděrových prostoročasech, Melnikovova metoda

Title: Geodesic chaos in a perturbed Schwarzschild field

Author: Lukáš Polcar

Institute: Institute of Theoretical Physics

Supervisor: doc. RNDr. Oldřich Semerák DSc., Institute of Theoretical Physics

Abstract: We study the dynamics of time-like geodesics in the field of black holes perturbed by a circular ring or disc, restricting to static and axisymmetric class of space-times. Two analytical methods are tested which do not require solving the equations of motion: (i) the so-called geometric criterion of chaos based on eigenvalues of the Riemann tensor, and (ii) the method of Melnikov which detects the chaotic layer arising by break-up of a homoclinic orbit. Predictions of both methods are compared with numerical results in order to learn how accurate and reliable they are.

Keywords: General relativity, geodesic deviation, chaos in black-hole space-times, Melnikov method

Contents

Introduction

The theory of dynamical systems, more commonly known as the chaos theory, is a relatively modern branch of mathematics which is applicable in many areas. Originally it was developed as a tool to study nonlinear systems in physics, especially in the context of classical mechanics. Actually, it has turned out that linear systems represent but tiny fraction of real physical and mathematical world, which indicates that in nature chaotic behaviour is a rule rather than an exception. The most intuitive aspect of chaos is a sensitive dependence on initial conditions, nowadays mainly popular from meteorology, but already for long known from the Newtonian gravity (the three-body system).

In this thesis, we will study several dynamical systems whose unperturbed configuration space is given by gravitational field of a black hole. Although we will partially resort to a (pseudo-)Newtonian treatment, it is clear that such an extreme strong-field object can only be properly described within Einstein's general theory of relativity which describes gravity geometrically as a curvature of spacetime. This theory – as opposed to Newton's theory – is non-linear, so one can expect that the dynamical systems which appear there will be even more prone to chaos.

According to the black-hole uniqueness theorems, every isolated stationary black hole in an otherwise regular asymptotically flat space-time is given by the Kerr-Newman solution, i.e., it is axially symmetric, it has a horizon of spherical topology and it is fully characterized by at most four parameters (of which physically relevant are three – mass, angular momentum and electric charge, and astrophysically only the first two). One of "miraculous" properties of the Kerr-Newman geometry is that (electro-)geodesic motion of test particles is completely integrable, so there is no room for chaos there. However, actually *any* perturbation of the Kerr-Newman geometry – typically due to the presence of some additional matter around – destroys this integrability (even if the perturbation keeps all the symmetries of the original space-time, namely stationarity, axisymmetry and reflectional symmetry). This feature, also surviving in the non-rotating, Schwarzschild or Reissner-Nordström case, is due to the existence of an unstable periodic (spatially circular) orbit and the attached homoclinic orbit. Such a situation is of course very interesting for theoretical study, but is is also important astrophysically, because almost all evidence for real black holes acquired so far is a consequence of their interaction with matter and fields around.

The only setting where one can hope to be able to treat, as an exact solution of Einstein's equations, the space-time of a black hole surrounded by an additional source, is just the stationary (even better static) and axially symmetric case. Fortunately, as results of gravitational attraction and centrifugal repulsion, the accretion inflows onto compact objects, which fuel many extremely energetic astrophysical sources (active galactic nuclei, X-ray binaries, gamma-ray bursts), *are* supposed to be roughly axially symmetric, and in first approximation they are also treated as quasi-stationary (their accretion time is much longer than the orbital period).

In this thesis we will resort to the simplest, *static* case, and will specifically study the free motion of test particles around a Schwarzschild black hole per-

turbed by either an inverted Morgan-Morgan thin disc or a Bach Weyl ring. Although the title of the thesis involves the Schwarzschild black hole, we will also study the same problem in the space-time of an extreme Reissner-Nordström black hole encircled by a Majumdar-Papapetrou ring. In that system, both the black hole and the ring are (extremally) charged, so there is an electromagnetic field around, but the dynamics of neutral particles is similar to the first, uncharged system. (Extremally charged bodies are not physically relevant, but the Majumdar-Papapetrou ring has, surprisingly, much more reasonable properties than the Bach-Weyl ring. In any case, we wanted to also study a different system in order to see how robust are the results obtained for the first one.)

We will study the above systems using two very different analytical methods which should theoretically be able to predict the occurrence of chaos without solving the equations of motion. The first method is the geometric criterion of chaos which builds on the fact that geodesics tend to diverge on surfaces of negative Gauss curvature: it consists in calculation of eigenvalues of a certain matrix given by the Riemann curvature tensor. The validity of this criterion is often being questioned, so it will be interesting to test it on our systems against numerical integration of the geodesic equation.

The main focus of this thesis is on the Melnikov method. In contrast to the geometric criteria, this method is rather well established, namely it is based on mathematical theorems. It attempts to determine whether the system exhibits the so called homoclinic chaos. This type of chaos occurs when an unperturbed system possesses a homoclinic orbit (also called separatrix) that breaks up under a perturbation, leading to the formation of a very complicated structure called homoclinic tangle. Such a circumstance can be "diagnosed" by the analytically computed Melnikov function: only in that case the latter has simple zero points. Again, we will compare the results of the Melnikov method will numerics.

The thesis is structured as follows: the first two chapters bring a necessary theoretical background, with chapter one summarizing the basic concepts of the chaos theory and chapter two dealing with static and axisymmetric (specifically, Weyl) spacetimes. The third chapter describes the geometrical criterion and confronts its predictions with numerical simulations. The fourth chapter does the same for the Melnikov method. Application of the methods to both the above black-hole systems is an original work; the main contribution of the thesis is a necessary re-formulation of the Melnikov method, which has been found thanks to a canonical transformation to the suitable action-angle variables.

1. Basics of the chaos theory

In this chapter I will briefly describe basic concepts and methods of the chaos theory which will be used in our study of the perturbed black hole system.
Let us consider a system with a finite number of degrees of freedom which is described by a system of N ordinary differential equations:

$$\dot{x} = F(x,t), \qquad x \in X \subset \mathbb{R}^N. \tag{1.1}$$

The continuous time evolution described by this equation can also be understood as a mapping of the space of states X on itself: $f^t : X \to X$, $x(t) = f^t(x)$, as it is in the discrete case:

$$x_{n+1} = F(x_n, n), \qquad x \in X \subset \mathbb{R}^N. \tag{1.2}$$

Chaos in a dynamical system is often being introduced in terms of sensitive dependence on initial conditions or exponential divergence of nearby trajectories but there is actually no universally accepted definition. One of popular definitions of chaotic behaviour is due to Devaney [1989]:

Definition 1. *Let X be a metric space. A continuous map $f : X \to X$ is said to be chaotic on X if:*

1. *f is topologically transitive, i.e., for every two open subsets $U_1, U_2 \subset X$ there exists a finite time t such that $f^t(U_1) \cap U_2 \neq \emptyset$.*
2. *Periodic points are dense in X: for every $x \in X$ and $\varepsilon > 0$ there exists a periodic point p: $\|x - p\| < \varepsilon$.*
3. *f is sensitively dependent on initial conditions on X, i.e., if there exists $\varepsilon > 0$ such that for each point $x \in X$ and $\delta > 0$ arbitrary small, there exists point y: $\|x - y\| < \delta$ and a finite time t such that $\|x(t) - y(t)\| > \varepsilon$.*

This definition is analogous for the systems with discrete evolution. It is interesting to remark that Banks et al. [1992] showed that for continuous f the sensitive dependence on initial conditions is a consequence of the first two points of the definition.

In the following parts concerning the chaos theory we follow mostly the books by Lichtenberg and Lieberman [1983,1992] and Wiggins [2000].

1.1 Hamiltonian systems and canonical transformations

From now on we will discuss systems that are Hamiltonian which means that our space of states X is the phase space and a point in X is described by a set of n canonical coordinates q_i and also by an equal number of conjugated canonical momenta p_i. The dynamics is encoded in the Hamilton function $H(q_i, p_i, t)$, with the evolution equations (1.1) now taking the form of Hamilton's equations:

$$\dot{q}_i = \frac{\partial H}{\partial p_i}, \qquad \dot{p}_i = -\frac{\partial H}{\partial q_i}, \tag{1.3}$$

or, in a more compact form,

$$\dot{x}(t) = J\mathrm{D}H(x,t), \tag{1.4}$$

where $x = (\boldsymbol{q}, \boldsymbol{p})$ and

$$J = \begin{pmatrix} 0 & I \\ -I & 0 \end{pmatrix}.$$

If we wish to transform coordinates on phase space while preserving the structure of Hamilton's equations (1.3), we have to perform the so called canonical transformation and here we will specifically use the technique of generating function F which relates the old momenta (q_i, p_i) with the new ones $(\bar{q}_i, \bar{p}_i)$. There are four types of generating functions but for our purposes we will stick to the generating function of the second type $F_2(q_i, \bar{p}_i, t)$. The transformation equations then read

$$p_i = \frac{\partial F_2}{\partial q_i}, \tag{1.5a}$$

$$\bar{q}_i = \frac{\partial F_2}{\partial \bar{p}_i}, \tag{1.5b}$$

$$\bar{H}(\bar{q}_i, \bar{p}_i, t) = H(q_i, p_i, t) + \frac{\partial}{\partial t} F_2(q_i, \bar{p}_i, t). \tag{1.5c}$$

Setting the new hamiltonian $\bar{H} = 0$ and denoting $S \equiv F_2$, equation (1.5c) leads directly to the Hamilton-Jacobi equation

$$H(q_i, \frac{\partial S}{\partial q_i}, t) + \frac{\partial S}{\partial t} = 0. \tag{1.6}$$

For a hamiltonian that is not an explicit function of time, the Hamilton-Jacobi equation takes the form

$$H(q_i, \frac{\partial S}{\partial q_i}) = E. \tag{1.7}$$

1.2 Integrable systems and action-angle coordinates

Integrable systems represent a small but significant subset of dynamical systems. To introduce them we first need the concept of integral of motion. A function on phase space $I(q_i, p_i)$ is an integral of motion if it is conserved along a trajectory, $I(q_i(t), p_i(t)) = \text{constant}$. If this condition reduces the effective dimension of the phase space by one, then $I(q_i, p_i)$ is called isolating integral of motion.

If a system with N degrees of freedom possesses N independent isolating integrals of motion $I_1, \ldots, I_N$, then the system is called completely integrable. By independent we mean that their pairwise Poisson brackets vanish, $\{I_i, I_j\} = 0$.

Integrable systems have many interesting properties. One of them is that the time-independent Hamilton-Jacobi equation (1.7) becomes separable, which

enables us to perform canonical transformation to the so-called action-angle coordinates. We search the solution of (1.7) in the form

$$S = \sum_{i=1}^{N} S_i(q_i, \alpha_1, \dots \alpha_N), \tag{1.8}$$

where α_i are the new momenta $\bar{p_i}$, and also $\dot{\alpha_i} = 0$. Equation (1.7) then splits into N equations

$$H_i(q_i, \frac{\partial S_i}{\partial q_i}) = \alpha_i, \qquad i = 1, \dots N. \tag{1.9}$$

This set of equations can be solved by quadrature, and from the knowledge of the generating function S we can use equations (1.5a) and (1.5b) to perform the canonical transformation.

Momenta α_i are integrals of motion, but we will pass to a more useful set of integrals called actions J_i which are uniquely related to α_i by functions $\alpha_i = \alpha_i(J_j)$, in addition we assume that the motion in the phase space is bounded. The momenta called actions are then defined by

$$J_i = \frac{1}{2\pi} \oint p_i \mathrm{d}q_i = \frac{1}{2\pi} \oint \frac{\partial S_i(q_i, \boldsymbol{\alpha})}{\partial q_i} \mathrm{d}q_i, \tag{1.10}$$

where the integration is taken along a complete time period of the motion. Thus after the canonical transformation we obtain a hamiltonian which is a function of actions J_i only, $H = H(\boldsymbol{J})$. The corresponding Hamilton equations are then trivial as is their solution,

$$\begin{aligned} J_i &= \text{constant}, \\ \theta_i &= \omega_i t + \beta_i, \end{aligned} \tag{1.11}$$

where the coordinates θ_i conjugated to the actions J_i are called angles and are periodic, $\theta_i \in (0, 2\pi)$.

Fixing the values of J_i now confines the motion to a subset of the original phase space X. If in addition this subset is compact and connected, it can be shown that it is diffeomorphic to the N-dimensional torus T^N which is parametrized by the angles θ_i. This is the statement of the Liouville-Arnold theorem which is described in more details in Wiggins [2000] . The constants ω_i are frequencies of the motion. If the ratios of all possible pairs of frequencies are rational ($\frac{\omega_i}{\omega_j} \in Q \ \forall \ i, j$), the motion is periodic and we speak of a resonance (the corresponding torus is called the resonant torus). In the nonresonant case the trajectories densely fill the invariant torus and the motion is called quasiperiodic.

Another important feature of completely integrable systems is that they do not exhibit chaotic behaviour. The phase space consists only of the invariant tori and all trajectories are regular.

Despite the fact that the integrable systems are rare, they are often used to approximate real processes within perturbation theory. If an integrable system is subject to a sufficiently small perturbation, then under certain conditions some of the invariant tori are preserved (the nonresonant ones), therefore regular motion is still present in some regions of the phase space, although the system is not integrable any more, this is the result of the KAM theorem which is described in Wiggins [2000].

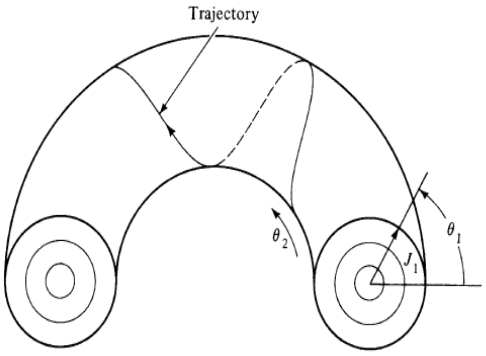

Figure 1.1: Illustration of an invariant torus (Merritt [1999]).

1.3 Numerical methods

In this section we will briefly discuss some tools that are often used in the numerical study of dynamical systems, the first being the Lyapunov exponents. Lyapunov exponents quantitatively describe the rate of divergence of two nearby trajectories. The exact definition is (under some assumption such as compactness of X)

$$\sigma(x_0, \boldsymbol{w}) = \lim_{t\to\infty} \lim_{d(0)\to 0} \frac{1}{t} \ln \frac{d(x_0, t)}{d(x_0, 0)}, \tag{1.12}$$

where $d = \|\boldsymbol{w}\|$, $\boldsymbol{w}$ being a deviation vector between two close trajectories in the phase space. This vector is a solution of variational equations which can be obtained by linearization of equations (1.1):

$$\frac{\mathrm{d}\boldsymbol{w}}{\mathrm{d}t} = \mathrm{D}F(x(t))\boldsymbol{w}, \tag{1.13}$$

where $\mathrm{D}F$ is the Jacobian matrix of F .

The Lyapunov exponent thus characterizes the evolution of the deviation vector $\boldsymbol{w}$ along trajectory $x(t)$. In fact we may consider, as the deviation vector, any of N vectors e_i that form a basis in the phase space, and consequently obtain N Lyapunov exponents σ_i. The trajectories are often said to be chaotic if at least one of the Lyapunov exponents is positive. Regular trajectories lying on the invariant tori have all $\sigma_i = 0$, for more details see Wiggins [2000] or Lichtenberg and Lieberman [1983,1992] .

Though the Lyapunov exponents are a widely used indicator of chaos, there are other quantities which characterize deviations of nearby trajectories, one of them being MEGNO (mean exponential growth of nearby orbits) which was introduced by Cincotta and Simó [2000]. MEGNO is defined as

$$Y(t) = \frac{2}{t} \int_0^t \frac{\dot{d}(s)}{d(s)} s \,\mathrm{d}s. \tag{1.14}$$

It is also useful to define the mean value of MEGNO,

$$\bar{Y}(t) = \frac{1}{t} \int_0^t Y(s) \,\mathrm{d}s. \tag{1.15}$$

The nature of a trajectory is given by the asymptotic behaviour of its averaged MEGNO. Writing this as

$$\bar{Y}(t) \approx at + b \text{ as } t \to \infty, \tag{1.16}$$

then for a chaotic trajectory $b = 0$ and a is proportional to the Lyapunov exponent σ; in the case of quasiperiodic motion $a = 0$ and $b = 2$, but the constant b may differ in some special situations of regular motion: for example, for a periodic trajectory one has $b < 2$.

The last method discussed here are Poincaré sections. Consider a system of two degrees of freedom which has an integral of motion $I(q_1, q_2, p_1, p_2)$. Then p_2 can be expressed as $p_2 = p_2(q_1, q_2, p_1)$, moreover we can reduce the effective dimension of the phase space even further by choosing a surface of section Σ given by equation $P_\Sigma(q_1, q_2, p_1) = 0$. Each time the trajectory crosses the surface of section, a point is recorded, so the continuous evolution becomes a discrete mapping $f : \Sigma \to \Sigma$.

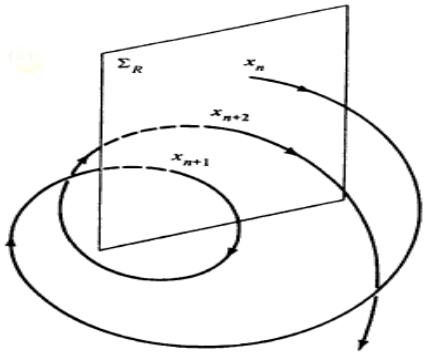

Figure 1.2: A trajectory intersecting a surface of section (from Coppo and Rougier [2012]).

The Poincaré section method is mostly used for a bounded motion and the section Σ is chosen so that the trajectories cross it repeatedly; one of natural choices of the surface is to set $q_2 =$ constant. The Poincaré section of a regular trajectory significantly differs from the chaotic one. Regular trajectories are confined to the invariant tori whose intersections with a surface of section results in continuous curves (which are present in the center of figure 1.3). In the special case of a periodic orbit the section consist only of a finite set of points. On the other hand, intersections of a chaotic trajectory densely fill out the corresponding Poincaré section, creating stochastic regions in the Poincaré map (which are marked by red in figure 1.3).

1.4 Homoclinic chaos

In this final part of the first chapter I will briefly indicate how some particular structure in the phase space affects the dynamics in its vicinity. This topic is discussed in much more detail in Wiggins [2000]. The basic results in this area are due to Poincaré, Birkhoff and lastly Smale who devised a famous chaotic map

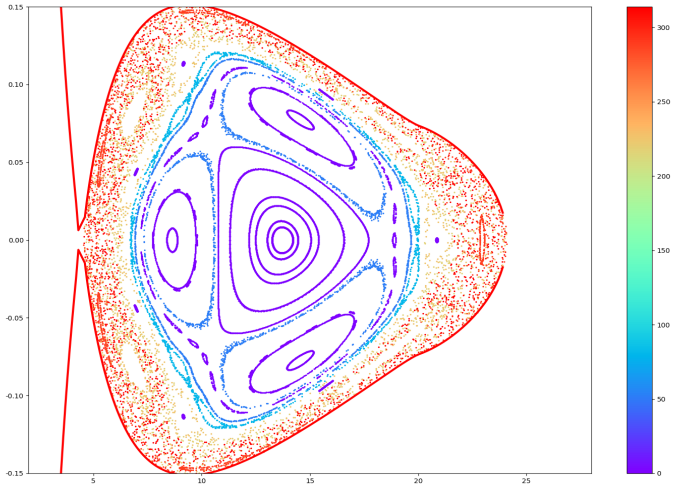

Figure 1.3: Example of a Poincaré section.

known as the Smale horseshoe and showed its relation to the dynamics near the so called homoclinic points.

Smale horseshoe (see figure 1.4) is a discrete mapping of a unit square on $\mathbb{R}^2$, $f : D \to \mathbb{R}^2$. The square is stretched, folded and finally laid on itself while some points leave the original square, so we are left with $f(D) \cap D$ which is represented by two vertical rectangles on each side of the square D. Similarly, the mapping f^{-1} can be defined as depicted in figure 1.4.

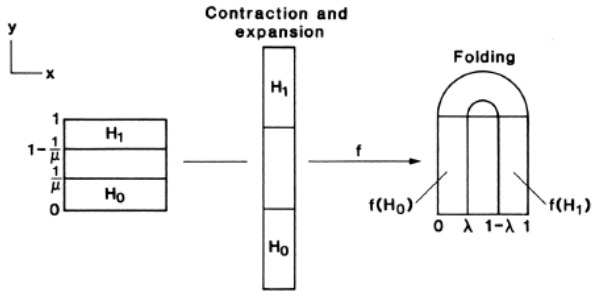

(a)

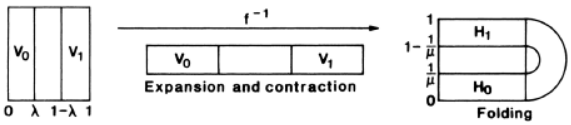

(b)

Figure 1.4: Two vertical rectangles correspond to $f(D) \cap D$ (a) and horizontal ones to $f^{-1}(D) \cap D$ (b) (from Wiggins [2000]).

After repeatedly applying f, we get $\bigcap_{n=0}^{N} f^n(D)$ which results in getting 2^N vertical strips as can be seen in figure 1.5. This can be repeated over and over (and also

in the reversed direction of mapping) until we get an invariant set of points which never leave the square D under the mapping f: $\Lambda = \bigcap_{n=-\infty}^{\infty} f^n(D)$. The set Λ is an invariant set of f and it can be shown that it is chaotic in nature. Additionally, a point $p \in \Lambda$ can be represented uniquely by an infinite sequence of numbers $s_i \in \{0, 1\}$,

$$p \mapsto s = \{\ldots s_{-n} \ldots s_{-1}.s_0 \ldots s_n \ldots\}, \tag{1.17}$$

where s_i is defined as $f^i(p) = H_{s_i}$ (H_0 and H_1 are the horizontal rectangles in figure 1.4). The assignment of a point to an infinite sequence s is also unique. The evolution of p is then just a shift of its infinite sequence,

$$f(s) = \{\ldots s_{-n} \ldots s_0.s_1 \ldots s_n \ldots\}. \tag{1.18}$$

From (1.17) we can deduce that f has two fixed points ($\{\ldots 00.0 \ldots\}$ and $\{\ldots 11.1 \ldots\}$) and an infinite number of periodic orbits of arbitrary long period (for example $\{\overline{010.101}\}$). This abstract mapping which uses two numbers $\{0, 1\}$ can be generalized to an N-symbol dynamics.

The most important property of this mapping is that it satisfies all three conditions of definition (1) and therefore it is chaotic. Without a rigorous proof we can look, for example, at the second condition which demands that periodic points are dense in X. In Λ each point can be approximated by a periodic point as closely as we want since we have periodic orbits of arbitrarily long period and thus the periodic points are dense in Λ. Similarly we can have two points with sequences s and $\tilde{s}$ with $s_i = \tilde{s}_i$ for i up to some very large N but for N itself we have $s_N \neq \tilde{s}_N$. So we have two points very close to each other which however after f^N are mapped into different rectangles (one point to H_0 the other to H_1), which indicate sensitive dependence on initial conditions.

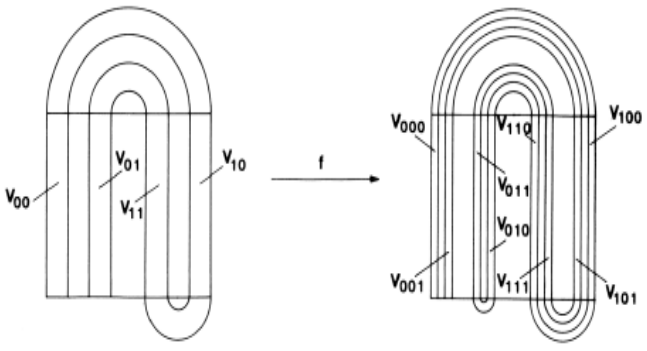

Figure 1.5: Second (left) and third (on the right) application of the mapping f. Reproduced from Wiggins [2000].

One would certainly ask what is the relation between the Smale chaotic map and the dynamics in classical (Hamiltonian) mechanics. The answer is that the link between the two lies in the concept of homoclinic points (orbits). Consider for simplicity a one-degree-of-freedom system described by hamiltonian $H(q, p, t)$ which is periodic in time ($t \in (0, T)$); this makes the phase space effectively three-dimensional. Then we take a surface of section Σ which turns the continuous

evolution into discrete mapping. Denoting $x(t) := (q(t), p(t))$ we define $x_0 = x(t_0)$ for some $t_0 \in (0, T)$ and subsequently $x_n = x(t_0 + nT)$. The mapping can now be written in the common form $x_{n+1} = f(x_n)$.

Next we make two key assumptions about $f : \Sigma \to \Sigma$:

1. f possesses an unstable (hyperbolic) fixed point p,
2. stable and unstable manifold $W^s(p)$ and $W^u(p)$ intersect transversally.

The term fixed point obviously means $f(p) = p$ and by hyperbolic or unstable we mean that the Jacobian matrix $\mathrm{D}f(p)$ has no eigenvalue with zero real part. The fixed point p corresponds to a periodic orbit with period T in the original three-dimensional phase space.

Finally we define stable and unstable manifolds and homoclinic points:

Definition 2. *Let $f : \Sigma \to \Sigma$ possesses a hyperbolic fixed point p. We define:*

1. *Stable manifold W^s to a hyperbolic fixed point p is a set $W^s(p) = \{x \in \Sigma, f^n(x) \to p \ \ as \ \ n \to \infty\}$.*
2. *Unstable manifold W^u to a hyperbolic fixed point p is a set $W^u(p) = \{x \in \Sigma, f^n(x) \to p \ \ as \ \ n \to -\infty\}$.*
3. *A point x is a homoclinic point if $x \neq p$ and $x \in W^s(p) \cap W^u(p)$.*

Both asymptotic manifolds are represented as continuous curves in the section Σ and two-dimensional surfaces in the original phase space X. As for the homoclinic points, if there is one homoclinic point, then there exist infinitely many of them. This is a trivial consequence of the definition. The trajectory corresponding to a homoclinic point is called the homoclinic trajectory.

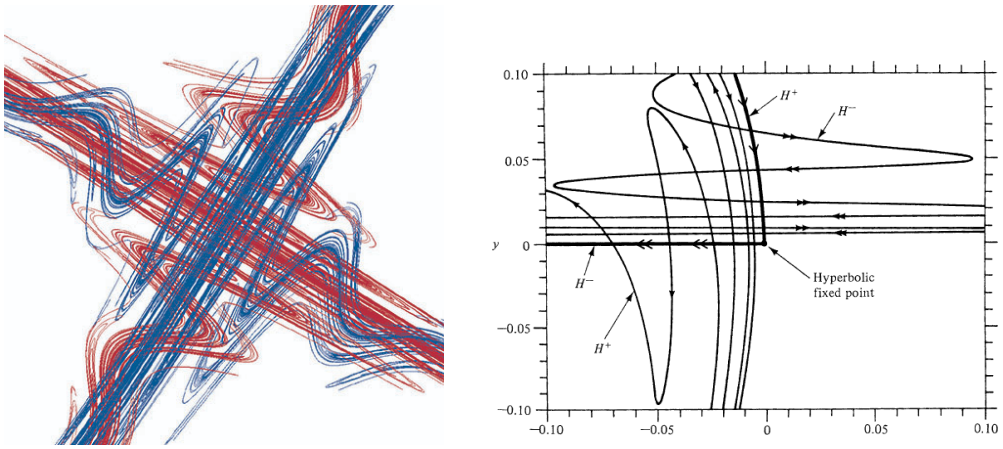

Figure 1.6: A homoclinic tangle (W^s and W^u intersect transversally). Left figure is reproduced from Sander and Yorke [2015],while the right one is from Lichtenberg and Lieberman [1983,1992].

Let us get back to the assumptions. In the second one transverse intersections are mentioned, by that we mean that for the sum of tangent spaces of the two manifolds it holds $T_x W^s + T_x W^u = T_x X$, the point x is then called transverse homoclinic point.

The set of all transverse homoclinic points is often called the homoclinic tangle and it has a very complicated structure (figure 1.6) since as we approach the hyperbolic fixed point we encounter more and more intersections. In fact the behaviour of the points in a close neighbourhood of homoclinic points is very similar to that of the points from the invariant set Λ of the Smale horseshoe which can be described by the infinite sequences of zeros and ones. The message of the previous sentence can be precisely stated as the Smale-Birkhoff homoclinic theorem:

Theorem 1.4.1 (**Smale-Birkhoff homoclinic theorem**). *Let $f : \mathbb{R}^2 \to \mathbb{R}^2$ be a C^r ($r \geq 1$) diffeomorphism satisfying assumptions 1 and 2. Then there exists an integer $n \geq 1$ such that f^n has an invariant Cantor set on which it is topologically conjugate to a full shift of N symbols.*

The theorem implies that in a close neighbourhood of a transverse homoclinic point the dynamics is chaotic; the whole derivation (proof) can be found in Wiggins [2000]. The horseshoe-like dynamics is illustrated in figure 1.7.

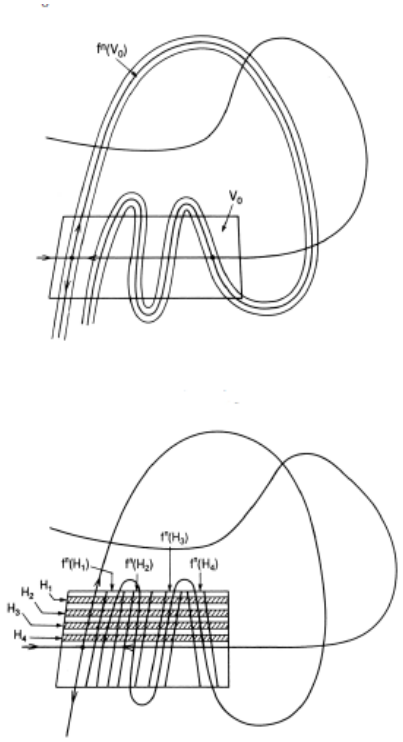

Figure 1.7: Horizontal strips mapped on themselves by a diffeomorphism f^n (from Wiggins [2000]).

To conclude the first chapter we make one important remark. The knowledge of existence of the transverse homoclinic orbits (points) does not tell how large the chaotic area in the phase space is. Instead we can only tell that chaotic regions are formed close to the homoclinic points and especially close to the unstable periodic orbit. Thus the motion sufficiently far from the whole homoclinic structure may remain completely regular (see Lichtenberg and Lieberman [1983,1992]). In fact in the near-integrable systems (integrable systems with a small perturbation) with homoclinic tangle, the chaotic regions are typically located only in a small

region close to the unperturbed separatrix (see section 4.1.) surrounded by KAM tori which actually fill most of the phase space (see figure 1.8).

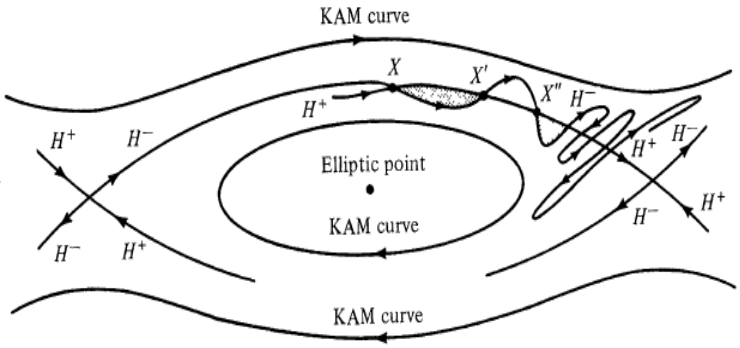

Figure 1.8: Homoclinic tangle confined in a small region surrounded by invariant KAM tori (Lichtenberg and Lieberman [1983,1992]).

The concept of transverse homoclinic intersection is central to the so called Melnikov's method which will be discussed in chapter 4.

2. Weyl spacetimes

In this chapter some basic properties of the Weyl spacetimes will be discussed with focus on the solutions of Einstein equations describing a static (and charged) black hole and infinitesimally thin discs or rings. More details on the general theory can be found in the book by Griffiths and Podolský [2009] while the particular solutions can be found in article by Semerák and Suková [2010].

2.1 Weyl metric

Weyl metrics represent a family of static and axisymmetric exact solutions of Einstein equations. A general form of the Weyl metric is

$$\mathrm{d}s^2 = -e^{2\nu(\rho,z)}\mathrm{d}t^2 + e^{2\lambda(\rho,z)-2\nu(\rho,z)}(\mathrm{d}\rho^2 + \mathrm{d}z^2) + \rho^2 e^{-2\nu(\rho,z)}\mathrm{d}\phi^2. \tag{2.1}$$

It is expressed in cylindrical-like coordinates called Weyl coordinates: $z, t \in \mathbb{R}$, $\rho \in (0, \infty)$ and $\phi \in (0, 2\pi)$, where $\rho = 0$ is the axis of symmetry. The symmetries of the metric are equivalent to the existence of two Killing vector fields, $\xi_{(t)} = \partial_t$ and $\xi_{(\phi)} = \partial_\phi$. The metric is determined solely by two functions: $\nu(\rho, z)$ and $\lambda(\rho, z)$. Vacuum Einstein equations with zero cosmological constant ($R_{\mu\nu} = 0$) reduce to

$$\nu_{,\rho\rho} + \frac{1}{\rho}\nu_{,\rho} + \nu_{,zz} = 0, \tag{2.2}$$

$$\lambda_{,\rho} = \rho\Big[(\nu_{,\rho})^2 + (\nu_{,z})^2\Big], \qquad \lambda_{,z} = 2\rho\nu_{,\rho}\nu_{,z}. \tag{2.3}$$

Equation (2.2) is just the Laplace equation in cylindrical coordinates which is linear and thus allows superposition of solutions exactly like in Newton's theory of gravity. The metric function ν plays the role of the Newtonian gravitational potential. Knowing ν, one can compute λ from equation (2.3) with a supplementary condition $\lambda = 0$ on the axis (see Griffiths and Podolský [2009] and Semerák and Suková [2010]).

The function ν can be taken from the Newton theory, but the corresponding complete solution (2.1) is often not a straightforward relativistic equivalent of its Newtonian counterpart. For example, taking the Newtonian solution for the particle of mass M located at the origin ($\nu = \frac{-M}{\sqrt{\rho^2+z^2}}$) and inserting it, together with the corresponding λ into the general form of the metric (2.1) leads to the Curzon-Chazy solution which is quite different from the expected Schwarzschild solution. Similarly, there are several Newtonian potentials that lead to a flat Minkowski spacetime (Griffiths and Podolský [2009]).

In the following parts we mention several specific Weyl-class solutions on whose backgrounds we will then study the motion of test particles.

2.2 The Schwarzschild solution

The Schwarzchild solution is one of the most famous solutions of the Einstein equations and also the first that can describe a black hole. It is a vacuum spherically symmetric solution with a single parameter M representing mass of the source. In the Weyl coordinates, the two metric functions read

$$\nu(\rho,z)=\frac{1}{2}\ln\left(\frac{d_1+d_2-2M}{d_1+d_2+2M}\right),\qquad \lambda(\rho,z)=\frac{1}{2}\ln\left(\frac{(d_1+d_2)^2-4M^2}{4d_1d_2}\right), \tag{2.4}$$

where $d_{1,2}=\sqrt{\rho^2+(z\mp M)^2}$. Schwarzschild solution is often expressed in the spherical-type (Schwarzschild) coordinates (t,r,θ,ϕ) as

$$\mathrm{d}s^2=-\left(1-\frac{2M}{r}\right)\mathrm{d}t^2+\frac{1}{1-\frac{2M}{r}}\mathrm{d}r^2+r^2(\mathrm{d}\theta^2+\sin^2\theta\,\mathrm{d}\phi^2). \tag{2.5}$$

The coordinate transformation between the Schwarzschild and Weyl coordinates reads

$$\rho=\sqrt{r^2-2Mr}\sin\theta,\qquad z=(r-M)\cos\theta. \tag{2.6}$$

The Weyl coordinates are useful for superposition of the Schwarzschild centre with an additional source (e.g. ring/disc) while the spherical-type coordinates are more suitable for example for some manipulations with hamiltonian which will be performed in chapter 4.

The metric (2.5) has two singularities, the first being a curvature singularity at $r=0$ and the other is a coordinate one at $r=2M$ which corresponds to a null hypersurface known as the event horizon. The Schwarzschild coordinates do not cover the entire spacetime manifold. The solution can be maximally extended using the Kruskal-Szekeres coordinates which also eliminate the horizon singularity. The Weyl coordinates describe even smaller part of the spacetime – the part above the horizon ($r>2M$), since it is a static region in contrast to the black hole itself. In Weyl coordinates the horizon is represented as a finite rod on the axis ($\rho=0,|z|<M$).

The motion of test particles around the Schwarzschild centre (e.g. a black hole) is different from the classical case. Famous is the perihelion precession of bound orbits but for us a more important feature is the existence of an unstable periodic orbit with a degenerate homoclinic orbit connected to it. These orbits are not present in the classical Kepler problem and may lead to a homoclinic chaos under perturbation (chapter 4).

The Schwarzschild black hole can be approximated using a pseudo-Newtonian potential in such a way that it reproduces some of its features (e.g. the homoclinic orbit) which would otherwise be lost if one reverted back to the Newton gravity. One such example is the Paczyński-Wiita (PW) potential which has the form

$$V_{PW}(r)=-\frac{M}{r-2M}. \tag{2.7}$$

Another example is the Nowak-Wagoner (NW) potential

$$V_{NW}(r)=-\frac{M}{r}\left(1-\frac{3M}{r}+\frac{12M^2}{r^2}\right). \tag{2.8}$$

The PW potential approximates the relativistic solution better then the NW potential nevertheless for our purposes the Nowak-Wagoner potential will be more useful in chapter 4. Witzany et al. [2015] studied the pseudo-Newtonian potentials with perturbations due to additional sources including comparisons with the motion in a fully relativistic system.

2.3 Inverted Morgan-Morgan disc

Inverted Morgan-Morgan (M-M) discs are a family of infinitely thin discs obtained by Kelvin transformation from the original M-M disc which have non-zero density for $\rho \in (0, b)$ in the equatorial plane (b is the disc radius). Inverting the disc with respect to $\rho = b$, one still gets a solution of Laplace equation but this time with $\rho \neq 0$ for $\rho \in (b, \infty)$. In our computations we will only study the first disc of the family with Newtonian density dependence

$$\omega = \frac{2mb}{\pi^2 \rho^3} \sqrt{1 - \frac{b^2}{\rho^2}}, \qquad \rho > b,\ z = 0, \tag{2.9}$$

where m is the total mass of the disc. The first metric function ν is

$$\nu(\rho, z) = -\frac{m}{\pi(\rho^2 + z^2)^{\frac{3}{2}}} \left[\left(2\rho^2 + 2z^2 - b^2 \frac{\rho^2 - 2z^2}{\rho^2 + z^2} \right) \operatorname{arccot}\left(\sqrt{\frac{\Sigma - (\rho^2 + z^2 - b^2)}{2(\rho^2 + z^2)}} \right) - (3\Sigma - 3b^2 + \rho^2 + z^2) \sqrt{\frac{\Sigma - (\rho^2 + z^2 - b^2)}{8(\rho^2 + z^2)}} \right] \tag{2.10}$$

where $\Sigma = \sqrt{(\rho^2 + z^2 - b^2)^2 + 4b^2 z^2}$.

The second metric function is known, analytically, for the disc alone, but not for its superposition with Schwarzschild, so we will have to find it numerically at each point.

Finally it is worth mentioning that due to having an infinitely thin disc the derivative $\frac{\partial \nu}{\partial z}$ at the points where the disc is located (equatorial plane) has discontinuity (jump) which may greatly affect the motion of test particles.

2.4 Bach-Weyl ring

Bach-Weyl ring is a counterpart of the Newtonian circular ring. The metric function ν is just the Newtonian potential for a ring in the equatorial plane,

$$\nu(\rho, z) = -\frac{2mK(k)}{\pi \sqrt{(\rho + b)^2 + z^2}}, \tag{2.11}$$

.

where $K(k)$ is the elliptic integral of the first kind,

$$K(k) = \int_0^{\frac{\pi}{2}} \frac{\mathrm{d}\phi}{\sqrt{1 - k^2 \sin^2 \phi}}, \qquad k = \sqrt{\frac{4\rho b}{(\rho + b)^2 + z^2}}.$$

Despite the fact that the solution describes "ordinary" ring in the Newton theory, its relativistic counterpart has some rather strange properties. For example, distance to the ring from a point in its interior ($\rho < b$) is infinite while from outer regions ($\rho > b$) it is finite. Also the proper time of flight to the ring is infinite for a point in the interior (for details see Semerák [2016]). This is an example that a solution which looks like a ring in cylindrical-like coordinates can have unexpected geometrical features.

2.5 The Majumdar-Papapetrou solutions

In the following, we will (also) consider solutions named after Majumdar and Papapetrou which form a subclass of the Weyl solutions. It is a class of electrovacuum solutions where the sources of the gravitational and electromagnetic field are extremally charged.

For the Majumdar-Papapetrou solutions of the Einstein-Maxwell equations, the second metric function is identically zero, $\lambda = 0$. The metric (2.1) can thus be rewritten using the lapse function $N = e^{\nu}$,

$$\mathrm{d}s^2 = -N^2\mathrm{d}t^2 + N^{-2}(\mathrm{d}x^2 + \mathrm{d}y^2 + \mathrm{d}z^2), \tag{2.12}$$

given by

$$\frac{1}{N} = 1 + \sum_{i=1}^{n} \frac{M_j}{|\vec{r} - \vec{r_i}|}. \tag{2.13}$$

The corresponding EM potential reads

$$A_\mu = (\pm N, 0, 0, 0).$$

The solution described by (2.13) can be interpreted as a superposition of n extremally charged static black holes with masses M_i and charges Q_i ($|Q_i| = M_i$) which are held in equilibrium since the electrostatic and gravitational forces cancel each other. The metric (2.12) is expressed in Cartesian-like coordinates which are related to the cylindrical-like coordinates in the same way as in the Euclidean space.

The simplest solution in this class is a single black hole located at the origin. The lapse function is then

$$\frac{1}{N} = 1 + \frac{M}{\sqrt{\rho^2 + z^2}}. \tag{2.14}$$

This is the extreme Reissner-Nordström black hole which can be described using spherical-like coordinates as

$$\mathrm{d}s^2 = -\left(1 - \frac{M}{r}\right)^2 \mathrm{d}t^2 + \frac{1}{(1 - \frac{M}{r})^2}\mathrm{d}r^2 + r^2(\mathrm{d}\theta^2 + \sin^2\theta\,\mathrm{d}\phi^2). \tag{2.15}$$

The coordinate transformation is similar to (2.6),

$$\rho = (r - M)\sin\theta, \qquad z = (r - M)\cos\theta. \tag{2.16}$$

The extreme Reissner-Nordström black hole has some similarities to the Schwarzschild solution. It possesses one degenerate horizon at $r = M$ but the region inside (the black hole itself) is static and the singularity is time-like in contrast to the Schwarzschild space-like singularity. The extremal Reissner-Nordström black hole also has a degenerate homoclinic orbit connected to an unstable periodic orbit.

If we arrange many such extreme black holes to a circle with radius b and make a continuous limit, we still obtain a solution of the field equations – the Majumdar-Papapetrou ring (MP ring), given by

$$\frac{1}{N} = 1 + \frac{2mK(k)}{\pi\sqrt{(\rho+b)^2+z^2}}. \tag{2.17}$$

The solution is expressed using the elliptic integral and the variable k as in the Bach-Weyl ring case. Though seeming rather artificial, this ring has more reasonable properties than the Bach-Weyl ring, mainly the distances and times of flight are finite no matter from which direction we approach the ring (Semerák [2016]). Thus this ring seems more realistic than the BW ring, which is also the reason why we will study the motion of test particles around it.

To conclude this section, we would like to mention that performing superposition within the Majumdar-Papapetrou class of solutions is trivial (see the expression for the lapse function (2.13)) which allows to combine the extreme Reissner-Nordström black hole with the MP ring in the following chapters. The electromagnetic four-potential (2.12) will not be important since we will consider neutral test particles.

2.6 Motion in the Weyl spacetime

Free test particles (i.e. particles interacting only with the gravitational field) in general relativity are moving along the so called geodesics which generalize the concept of straight lines from the Euclidean space to a curved spacetime.

In this thesis we will only deal with time-like geodesics which can be parametrized using proper time τ. For a given affine connection, the geodesic $x(\tau)$ can be found by solving the geodesic equation:

$$\frac{\mathrm{d}^2x^\mu}{\mathrm{d}\tau^2} + \Gamma^\mu_{\nu\rho}\frac{\mathrm{d}x^\nu}{\mathrm{d}\tau}\frac{\mathrm{d}x^\rho}{\mathrm{d}\tau} = 0. \tag{2.18}$$

In the Weyl spacetimes, the existence of the two Killing vectors leads to the conservation laws and thus allows us to reduce the dimension of the phase space. Specifically, the quantities conserved along geodesics are the projections of the particle four-momentum p_μ on the respective Killing fields,

$$\xi^\mu_{(t)}p_\mu = p_t = -E, \qquad \xi^\mu_{(\phi)}p_\mu = p_\phi = L_z. \tag{2.19}$$

They represent the particle energy and azimuthal angular momentum with respect to infinity. Thanks to these two integrals of motion and the normalization of the four-momentum ($p^\mu p_\mu = -m_0^2$) the 8-dimensional phase space is reduced to three dimensional one described by coordinates (r, θ, p_r) or (ρ, z, p_ρ).

Many systems in classical mechanics can be described using the Hamiltonian formulation. Hamiltonian of a freely falling particle with rest mass m_0 in general relativity is:

$$H = \frac{1}{2m_0} g^{\mu\nu}(x^\alpha) p_\mu p_\nu. \tag{2.20}$$

The corresponding Hamilton equations for the variables (x^μ, p_ν) are in fact the geodesic equations (2.18). The Hamiltonian formulation will play a key role in chapter 4.

3. Geometric criterion of chaos

The geometric criteria of chaos were the central topic of my bachelor thesis and because of that it will be covered here only briefly and the main focus will be on numerical tests of this method.

3.1 Description of the method

The geometric criterion is an analytical method attempting to find a connection between the motion of test particles in a given spacetime and the curvature of that spacetime. It attempts to study the motion in a gravitational system by plotting a map of unstable regions and based on how much of the accessible region they occupy it concludes whether the dynamics is regular or chaotic.

Our main reference is the article by Sota et al. [1996] which also deals with vacuum Weyl spacetimes. We have also used some insights into this method from Szydłowski [1994].

Consider two nearby geodesics connected by an infinitesimal deviation vector n^μ. Then the time evolution of this vector along a geodesic is governed by the geodesic deviation equation

$$\frac{\mathrm{D}^2 n^\mu}{\mathrm{d}\tau^2} = -R^\mu{}_{\nu\rho\sigma} u^\nu n^\rho u^\sigma. \tag{3.1}$$

This equation tells us that the relative acceleration of two close point particles is proportional to the curvature which is represented by the Riemann tensor on the right-hand side. The deviation vector can be chosen so that it is orthogonal to the four-velocity, $n_\mu u^\mu = 0$.

Assume we have an orthonormal basis $\{e^\mu_{(\nu)}\}$ ($u^\mu = e^\mu_{(0)}$) that is parallel-propagated along our geodesic ($\frac{\mathrm{D}e^\mu_{(\nu)}}{\mathrm{d}\tau} = 0$). Then in this basis the equation for vector $n^\mu = n^{(i)} e^\mu_{(i)}$ takes the form

$$\frac{\mathrm{d}^2 n^{(i)}}{\mathrm{d}\tau^2} = -R^{(i)}{}_{\nu(j)\sigma} u^\nu n^{(j)} u^\sigma. \tag{3.2}$$

Thus we have expressed the geodesic deviation equation in the basis $\{e^\mu_{(\nu)}\}$ replacing the absolute derivative with the total derivative with respect to the proper time. We can continue by transforming the equation to a gradient form

$$\frac{\mathrm{d}^2 n^{(i)}}{\mathrm{d}\tau^2} = -\mathrm{grad}^{(i)}_n V_u(n), \tag{3.3}$$

where the gradient is defined as $\mathrm{grad}^{(i)}_n = \frac{\partial}{\partial n^{(i)}}$ (we do not have to distinguish between upper and lower indices since the basis is orthonormal, $n^{(i)} = n_{(i)}$). The function $V_u(n)$ can be called potential and it is a quadratic form in n,

$$V_u(n) = \frac{1}{2} R_{(i)\nu(j)\sigma} n^{(i)} u^\nu n^{(j)} u^\sigma = \frac{1}{2} R(n, u, n, u). \tag{3.4}$$

In this way the geodesic deviation equation can be thought of as an equation for a fictitious particle moving in the potential $V_u(n)$. If $V_u(n)$ behaves like a potential

well, then the two neighbouring particles converge (more precisely the fictional particle would oscillate in the well), whereas if it is more like a potential hill, then the particles diverge from each other exponentially.

The behaviour described above is only local as the potential $V_u(n)$ changes along the geodesic since it depends on the four-velocity u^μ and also on the spacetime coordinates x^μ so the evolution of the deviation vector is rather complicated. As already mentioned, the potential is a quadratic form and to determine its behaviour we have to investigate the eigenvalues of the corresponding matrix $A^{(i)}{}_{(j)}$:

$$V_u(n) = \frac{1}{2} n_{(i)} A^{(i)}{}_{(j)} n^{(j)}, \qquad A^{(i)}{}_{(j)} = R^{(i)}{}_{\nu(j)\sigma} u^\nu u^\sigma. \tag{3.5}$$

It is clear that the 3×3 matrix $\mathbb{A}$ has three eigenvalues, but they depend on the four-velocity u^μ which we do not know as it requires solving the equations of motion. We would like to obtain some information solely from the curvature represented by the Riemann tensor which leads to a bivector formalism.

Let us define an antisymmetric tensor

$$S^{\mu\nu} = n^\mu u^\nu - u^\mu n^\nu. \tag{3.6}$$

This tensor (bivector) has six independent components and can be written as a column vector. This allows us to use the (anti)symmetries of the Riemann tensor to rewrite it as an 6×6 matrix on the space of bivectors in such a way that

$$R(n,u,n,u) = R_{\mu\nu\rho\sigma} n^\mu u^\nu n^\rho u^\sigma = \frac{1}{4} R_{\mu\nu\rho\sigma} S^{\mu\nu} S^{\rho\sigma} = R_{AB} S^A S^B, \tag{3.7}$$

where the index $A = 1 \dots 6$ is related to the Weyl coordinates as $S^1 = S^{t\rho}$, $S^2 = S^{tz}$ and so on, and the matrix R_{AB} corresponds to the Riemann tensor in the same way. We can now search for a solution of the eigenproblem

$$R^A{}_B S^B = \kappa S^A. \tag{3.8}$$

There are in total six eigenvalues κ_i of the Riemann-tensor matrix and it can be shown that up to some factor they are identical to the eigenvalues of the matrix $\mathbb{A}$ for some fixed four-velocity u^μ. This gets us back to our original problem of motion in the potential (3.5) and allows us to find eigenvalues of $\mathbb{A}$ independently of the four-velocity.

In this thesis we will apply the above method to the vacuum Weyl spacetimes (Schwarschild + BW ring/MM disc) and subsequently to the electrovacuum Majumdar-Papapetrou solution (extreme RN black hole + MP ring). The sum of the eigenvalues κ_i is proportional to the scalar curvature which is zero in both vacuum and electrovacuum spacetimes, so we have

$$\sum_{i=1}^{6} \kappa_i = 0. \tag{3.9}$$

Now, if we compute the Riemann tensor for a general Weyl metric (2.1), we find that $R^A{}_B$ is a block-diagonal matrix,

$$R = \begin{pmatrix} R_1 & 0 \\ 0 & R_2 \end{pmatrix}. \tag{3.10}$$

In the vacuum case it is even simpler (see Sota et al. [1996]) since $R_1 = R_2$ and therefore there are only three independent eigenvalues. Hence, we have three eigenvalues whose sum is equal to zero. If an eigenvalue is negative, its respective eigenvectors oscillate. If an eigenvalue is positive, the particles can diverge from each other. Thanks to their sum being zero, we can either have two negative eigenvalues and one positive, or two positive eigenvalues and one negative. The latter case can be called unstable region as geodesics tend to diverge from each other there. There are only two types of unstable regions since it turns out that the first of the eigenvalues is always positive which stems from the explicit calculation of the eigenvalues. So the two regions can be denoted as $(++-)$ and $(+-+)$ and the map of the two regions simply means plotting the inequalities $\kappa_2(x^\mu) > 0$ for $(++-)$ and $\kappa_3(x^\mu) > 0$ for$(+-+)$. The presence of these unstable regions should make the motion in the system chaotic according to this geometric criterion.

Similar but slightly more difficult is the application to the electrovaccuum spacetime. In that case $R_1 \neq R_2$, but by plotting the regions $\kappa_i > 0$ it turns out that the regions $\kappa_1 > 0$ and $\kappa_4 > 0$ nearly coincide; the same can be said for $\kappa_2 > 0$ and $\kappa_5 > 0$, and also for the last pair $\kappa_3 > 0$ and $\kappa_6 > 0$. Thus we can ignore the eigenvalues κ_4, κ_5 and κ_6 and be left with only three eigenvalues whose sum is approximately equal to zero and the mapping of the unstable regions is effectively the same as in the vacuum spacetimes.

When applying this criterion, a problem may arise due to the difficulty of finding the second metric function $\lambda(\rho, z)$ for the superposition of a black hole with a disc/ring. Fortunately, the function λ only appears in an exponential function which sits in front of the whole expression for the eigenvalue, and therefore it does not affect the sign of the eigenvalue. And the derivatives of λ can be expressed using the derivatives of ν according to equation (2.3).

Finally, let us mention yet another possible look at the geodesic deviation equation (3.1). This equation shows how the deviation vector connecting two infinitesimally close geodesics evolves in time. On the level of the phase space, this is described by the variational equation (1.13). These two equations are thus equivalent, actually there is a simple connection between them. Denoting $\xi = \frac{\mathrm{d}n}{\mathrm{d}\tau} = \dot{n}$, $\xi \in \mathbb{R}^3$ and using the 3×3 matrix $\mathbb{A}$ defined above and the unit matrix I, the variational equation can be written using a block matrix

$$\begin{pmatrix} \dot{n} \\ \dot{\xi} \end{pmatrix} = \begin{pmatrix} 0 & I \\ -\mathbb{A} & 0 \end{pmatrix} \begin{pmatrix} n \\ \xi \end{pmatrix}. \tag{3.11}$$

The matrix has six eigenvalues which can be expressed using the eigenvalues of the Riemann tensor matrix (3.8), namely they are given by $\pm\sqrt{\kappa_i}$, $i = 1 \ldots 3$. Divergence of the orbits can only occur for a positive eigenvalue while the negative leads to a harmonic oscillation as the eigenvalues of the variational-equation matrix are imaginary. Thus our eigenvalue analysis is the same as in any mechanical system described by the set of ordinary differential equations (1.1).

3.2 Testing the geometric criterion

As we have seen the outcome of the geometric criterion is the "prediction" map of unstable regions. The map has to be overlapped with the allowed region, because an unstable region outside the allowed region cannot affect the motion of test particles.

The allowed region can be found using the effective potential. The normalization of four-velocity in the Weyl metric can be rewritten as

$$g^{\rho\rho}(u_\rho)^2 + g^{zz}(u_z)^2 = e^{-2\nu(\rho,z)}(E^2 - V_{\text{eff}}(\rho, z)) \geq 0, \tag{3.12}$$

where the effective potential reads

$$V_{\text{eff}}(\rho, z) = e^{2\nu(\rho,z)}\left(1 + \frac{(L_z)^2}{\rho^2 e^{-2\nu(\rho,z)}}\right). \tag{3.13}$$

Thus plotting the inequality $E^2 - V_{\text{eff}}(\rho, z) \geq 0$ yields the allowed region in the Weyl coordinates. The allowed region in the spherical-like coordinates can be obtained by the transformations (2.9) or (2.16).

The predictions of the geometric criterion will be compared to the numerical simulations of geodesics. For this purpose we use the code by Miroslav Žáček. From the data obtained by this code we compute the MEGNO chaotic indicator and plot the Poincaré sections of our orbits using the scripts by Petra Suková. The surface of section is always the equatorial plane ($\theta = \frac{\pi}{2}$) and so the reduced phase space depicted in the Poincaré sections will be described by the coordinates (r, u^r). Each Poincaré section corresponds to a set of fixed parameters: the disc/ring mass m and radius b, and geodesic integrals of motion E and L_z. All particles start in the equatorial plane but with different coordinates (r, u^r). The map of unstable regions will be plotted in the Weyl coordinates. The orbits in the Poincaré sections are coloured (from blue to red) according to their reached value of MEGNO.

We start with the extreme Reissner-Nordström black hole surrounded by the Majumdar-Papapetrou ring. To be more precise we will study how the Poincaré section and the unstable-region map change with the particle energy. This is shown in figure 3.1. In this series we can see both types of unstable regions (marked by orange and blue) and the allowed region (red). For low energies most of the allowed region is occupied by unstable regions. The allowed region grows with energy while the unstable regions remain the same. This should lead to diminution of chaotic regions in the Poincaré sections. This actually happens in the series of figures 3.1, though not as significantly as we would expect (for example in the last figure (l)).

Another series (figure 3.2) illustrates the dependence of the geodesic dynamics on the ring radius b for the superposition of the Schwarzschild black hole and the Bach-Weyl ring. Here the connection between the unstable maps and the Poincaré section is more pronounced. As the radius grows, the unstable regions leave the allowed region which eventually splits into two parts (figure 3.2 (i)) with one part completely free of any unstable region while the other almost coinciding with one of unstable regions. This perfectly corresponds to the Poincaré sections on the right (3.2 (j)) where the region on the left is filled by smooth curves (tori intersections) while the other contains only a chaotic sea.

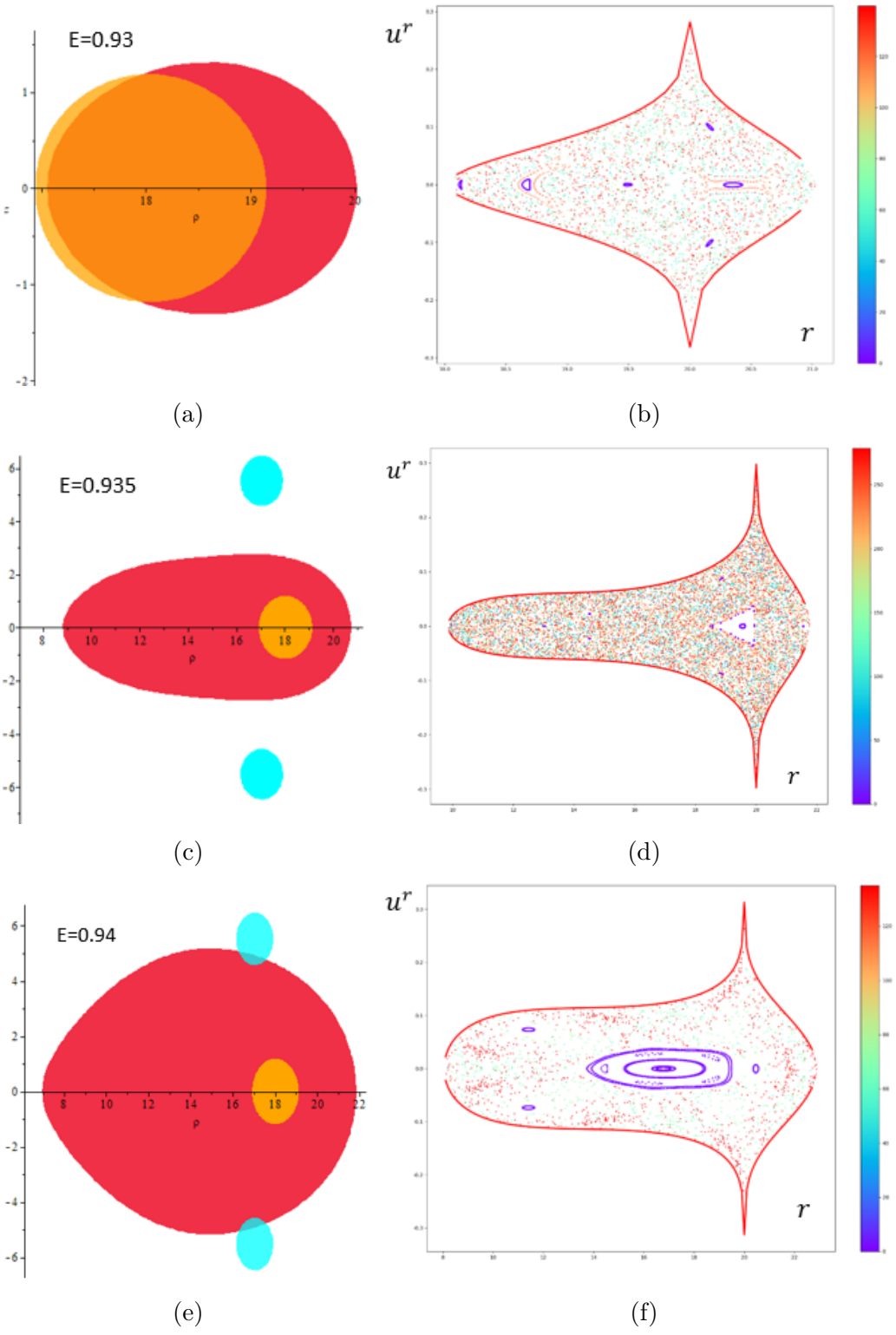

Figure 3.1: Unstable-regions maps and Poincaré sections for the extreme RN black hole with the MP ring. The dependence on energy is shown ($m = 0.5M$, $b = 20M$, $L_z = 3.75M$).

It thus seems that the geometric criterion works quite well, which means that it can predict the existence of chaotic regions. Similar results can be obtained for a series with changing mass of the ring/disc. A more complete analysis of

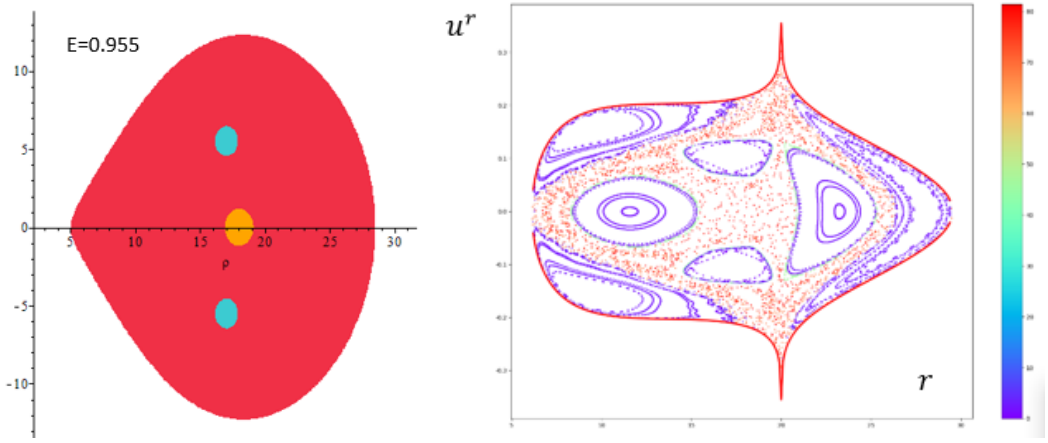

(g) (h)

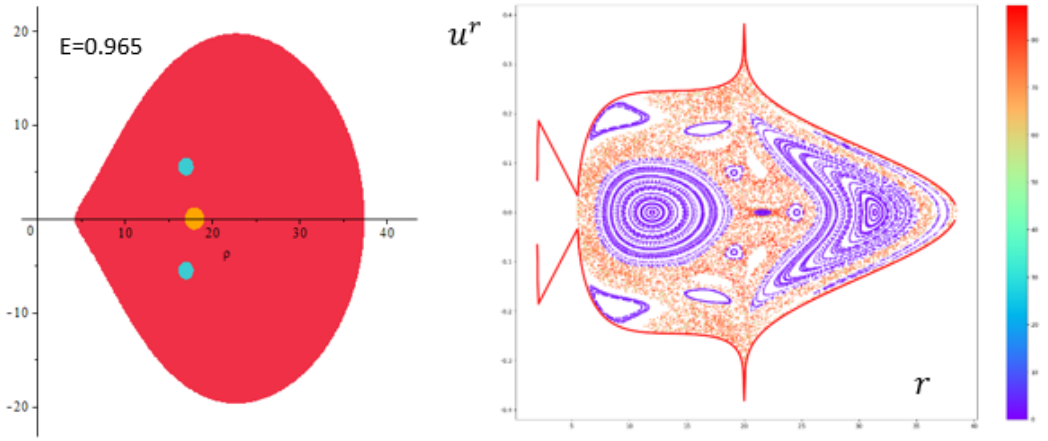

(i) (j)

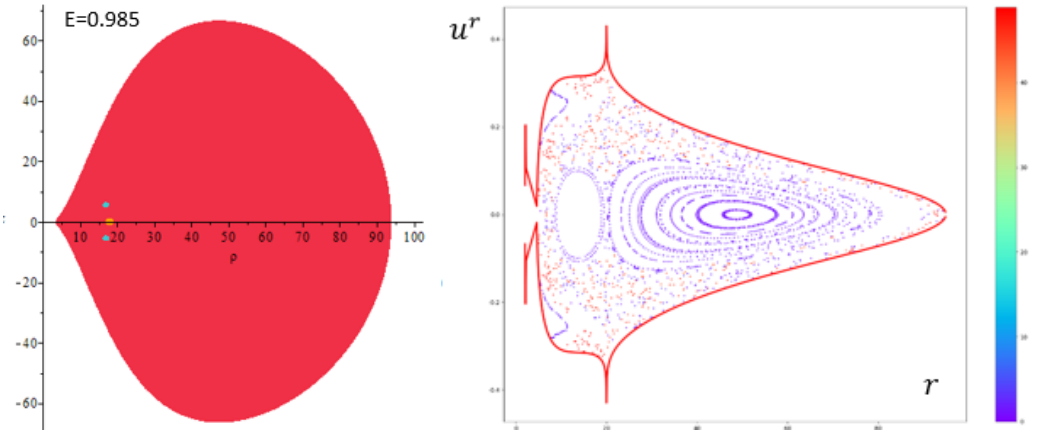

(k) (l)

Figure 3.1: continuation

the parameter dependence can be found in my bachelor thesis and so I will not discuss it further here.

We have not studied the case with the inverted Morgan-Morgan disc in detail yet, but it seems that the geometric criterion is not as effective as in the case of ring perturbations. One of the "counterexamples" is depicted in figure 3.3: the unstable region is completely outside of the allowed region and yet we can clearly

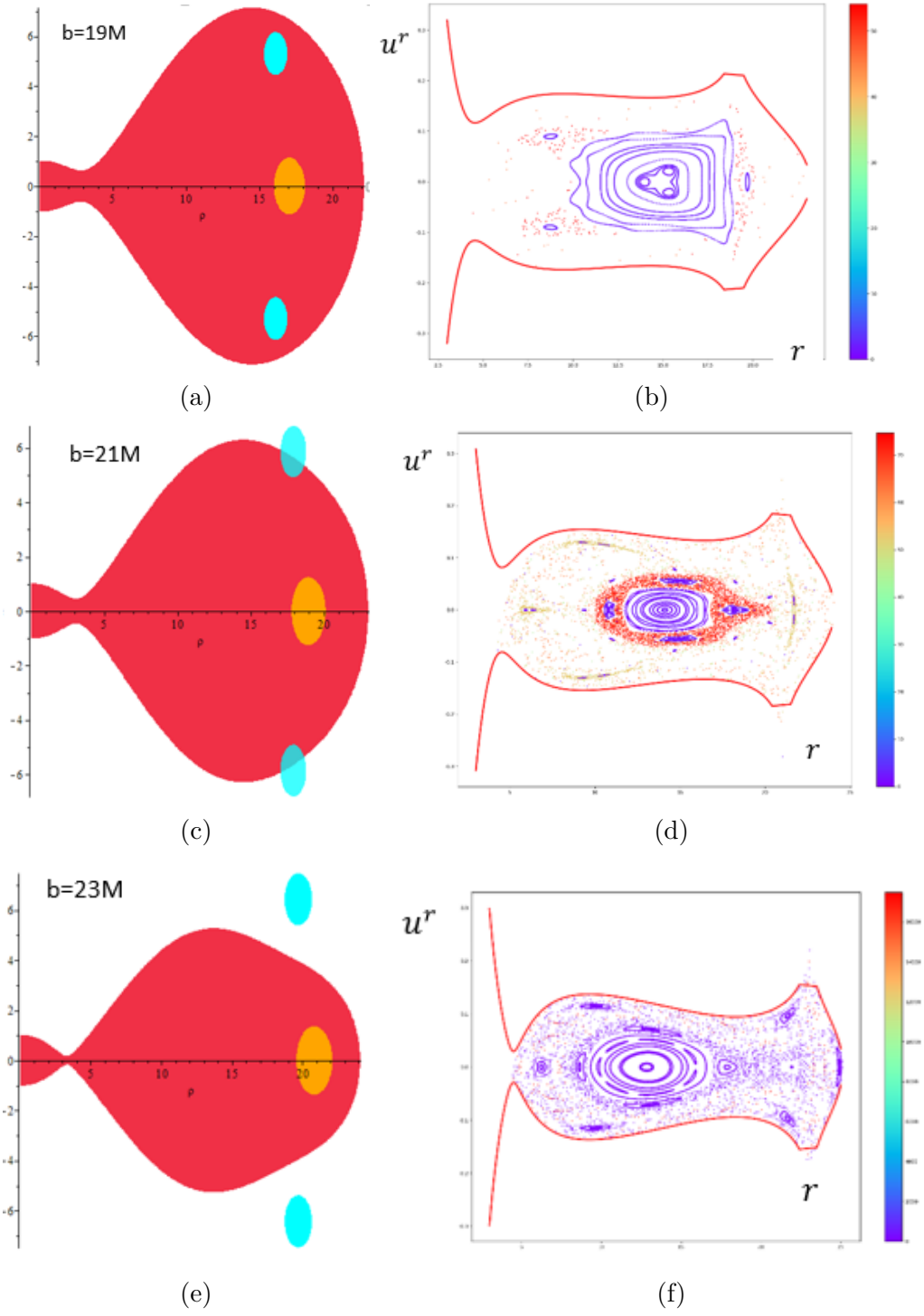

Figure 3.2: Unstable-region maps and Poincaré sections for the Schwarzschild black hole surrounded by the Bach-Weyl ring ($m = 0.5M$, $E = 0.94$, $L_z = 3.75M$). The dependence on the ring radius is shown.

see some chaotic orbits marked by the orange color in the corresponding Poincaré section.

The probable explanation of this failure of the geometric criterion is the fact that the particles cross the disc where the metric has discontinuous derivatives. We shall come back to this issue later.

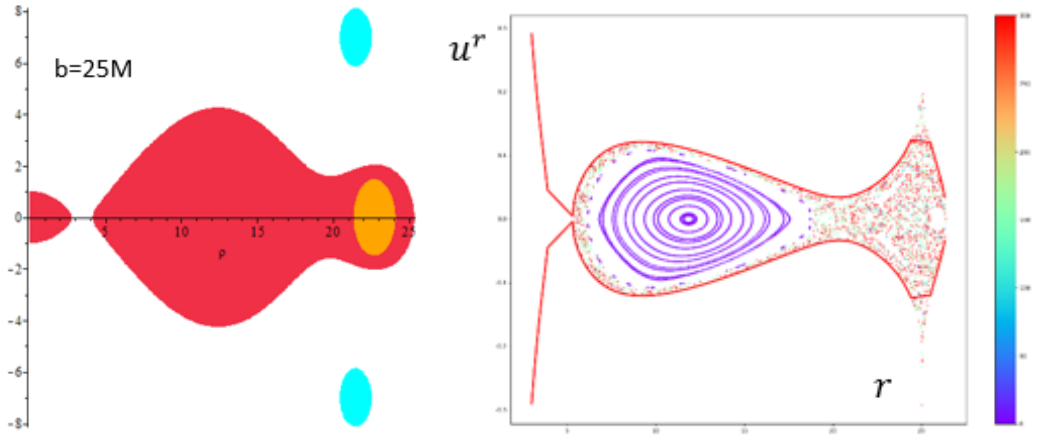

(g) (h)

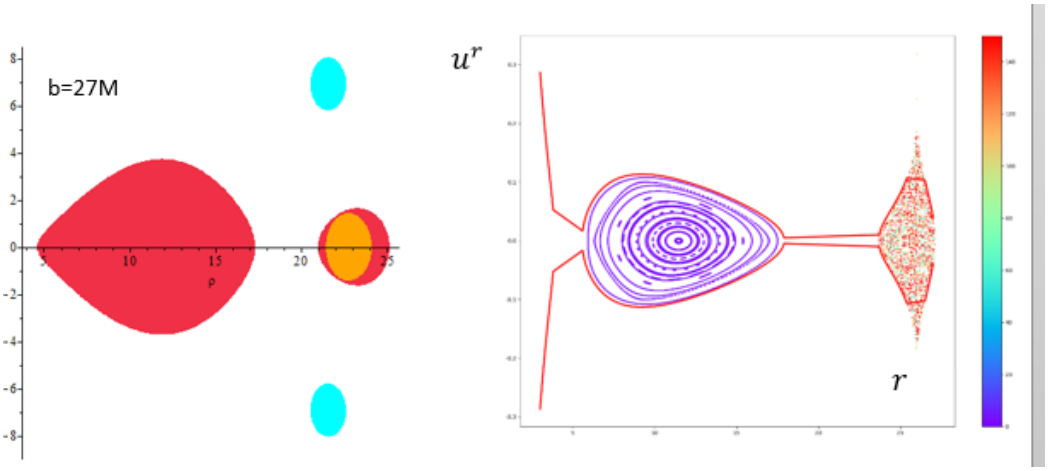

(i) (j)

Figure 3.2: continuation

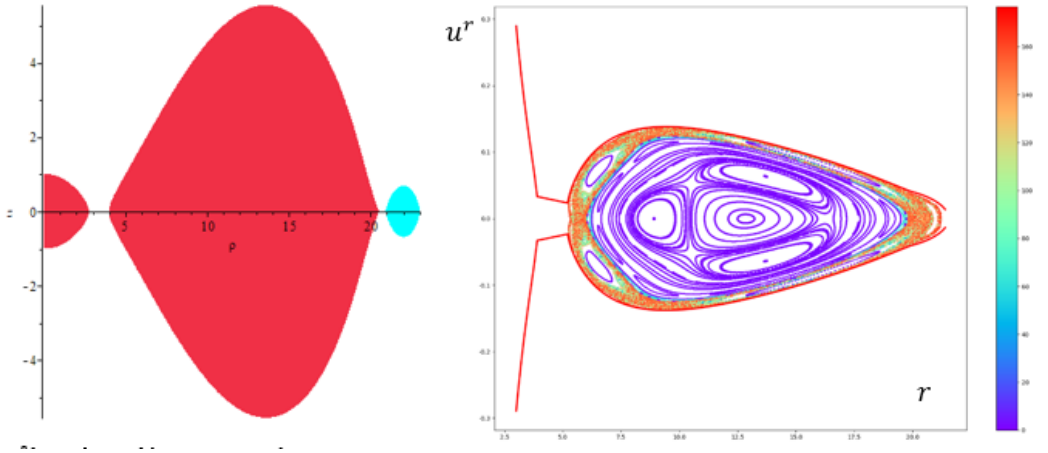

(a) (b)

Figure 3.3: Unstable-region maps and Poincaré sections for the Schwarzschild black hole surrounded by the first inverted Morgan-Morgan disc ($m = 0.5M$, $b = 20M$, $E = 0.953$, $L_z = 3.75M$).

Poincaré sections actually are not a sufficient tool to properly test the geometric criterion. As was already mentioned, the idea behind the criterion is that geodesics passing through the unstable regions diverge from each other. So the unstable regions should affect only those geodesics which pass through them while other geodesics should remain regular. To test this properly I used the scripts by Petra Suková to compute the MEGNO indicator and also my own code which records the proper time spent by a particle in the unstable regions. This enables one to test whether our understanding of the local interaction with the unstable regions is correct. We first give some examples of particular geodesics and then we will sum up the whole criterion by plotting a graph of dependence of MEGNO MG on the time τ spent in the unstable regions. For τ we can use absolute time spent inside the unstable regions τ_{in} or a ratio of this time relative to the entire time of simulation, $\tau_{\text{rel}} = \frac{\tau_{\text{in}}}{\tau_{\text{tot}}}$. Another option is the number of passages through the unstable regions. We observe that the use of all these options leads more or less to the same results.

Figure 3.4 shows the cases in which the criterion predicts regular or chaotic dynamics accurately. Most of the chaotic orbits were passing through the unstable regions regularly and their MEGNO grew steadily. Some regular orbits also spent certain time in the unstable regions but it was generally less than in the chaotic case.

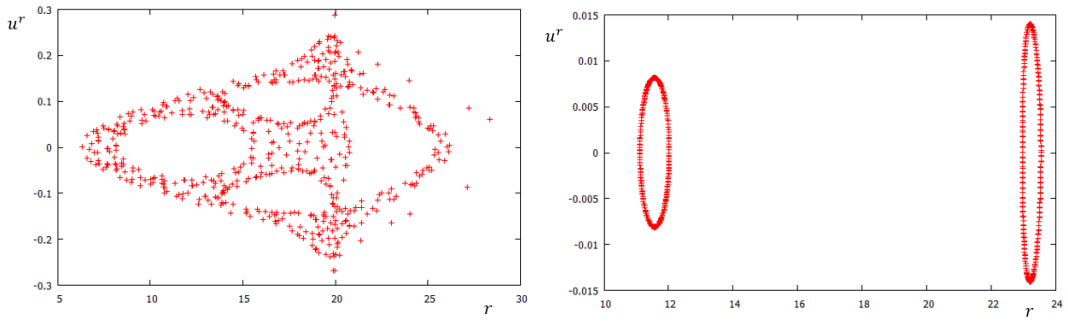

(a) (b)

Figure 3.4: Poincaré sections: (a) chaotic orbit ($MG = 41.44$, $\tau_{rel} = 0.0285$), (b) regular orbit ($MG = 1.39$, $\tau_{rel} = 0$).

An interesting case are orbits which start in the part of spacetime with no unstable regions but then, after some time, move to the part with unstable regions. An example of such a geodesic can be seen in figure 3.5 showing the map of unstable region (a), the dependence of MEGNO on time and the Poincaré section before (c) and after entering the unstable region (d). In the Poincaré section the orbit first produces a smooth curve, while after it enters the unstable region, it starts filling the plot densely, which supports the validity of the geometric criterion. This is also in accordance with the sudden growth of MEGNO in figure 3.5 (b).

It thus seems that the geometric criterion works quite well, however there are some orbits that contradict it. One of them can be seen in figure 3.6. It is clearly a regular orbit, but the MEGNO asymptotics indicates that it is probably close to some hyperbolic orbit ($MG = 3.054$). In spite of that, this orbit spends quite some time in the unstable region, even longer than the orbit in figure 3.4 (a)

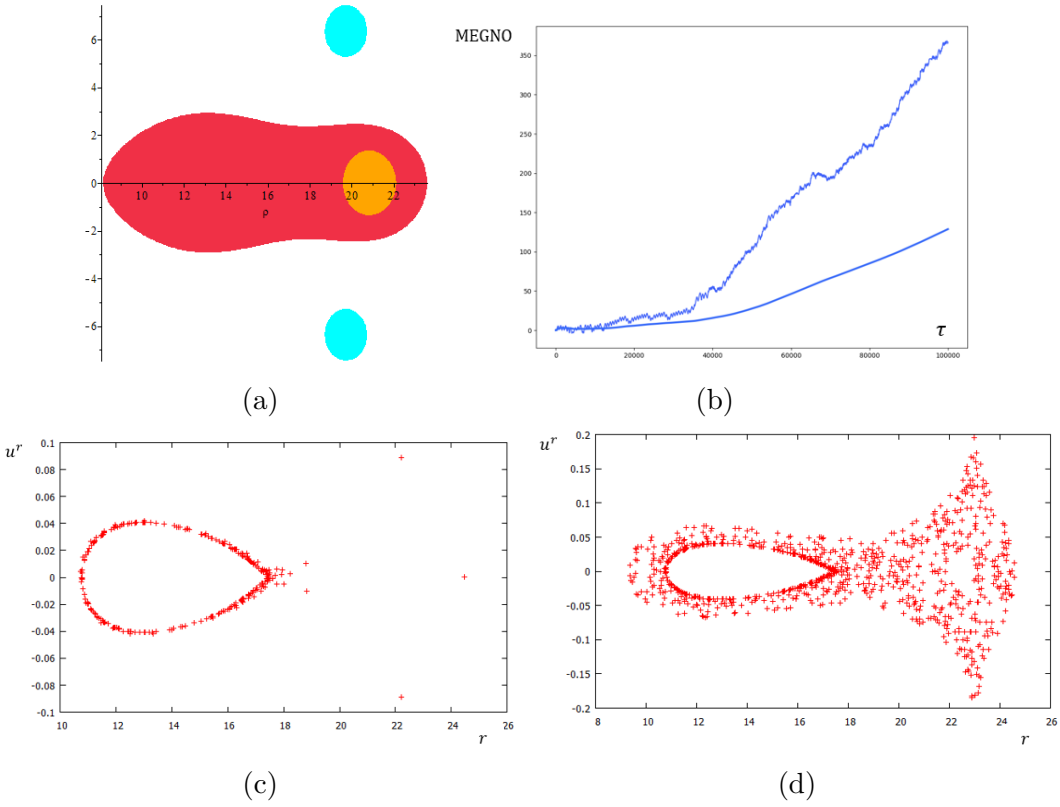

Figure 3.5: Map of unstable regions (a) and evolution of MEGNO (b) for orbit before (c) and after entering the unstable region (d).

which is described by the same set of parameters (and integrals of motion).

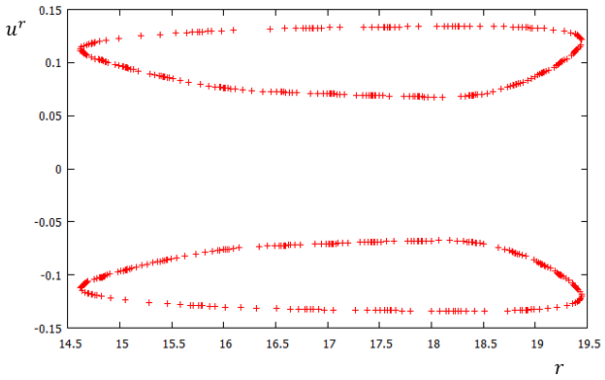

Figure 3.6: Poincaré section corresponding to a regular orbit with $MG = 3.054$, $\tau_{\text{rel}} = 0.0323$.

The cases when the geometric criterion fails are often (not always) those of regular trajectories where however the averaged MEGNO asymptotics is a constant deviating from the value of 2, which is typical for quasiperiodic motion. These orbits should be close to the resonant or hyperbolic torus according to the MEGNO theory (see article by Maffione et al. [2011]). So it may be that these particular structures in the phase space are unaffected by the presence of unstable regions.

What we can add is to summarize the results of the method for the MP and

BW ring in a single figure. We would naturally expect that the reached value of MEGNO should grow with time spent in the unstable regions. The resulting figure 3.7 gives us the answer. The MEGNO indeed grows with the number of passages, but there exist orbits with very long time spent in the unstable region and simultaneously very low MEGNO. These are the orbits already mentioned above (figure 3.6).

So the final conclusion based on all simulations I have performed is that for the superposition of the Schwarzschild black hole and the BW ring and also for the superposition of the extreme RN black hole and the MP ring the repetitive passages through the unstable regions is necessary for the geodesic to be chaotic. Thus in this case the geometric criterion is a necessary (but not sufficient) condition for the chaos to appear. There is however no rigorous proof for any of these assertions.

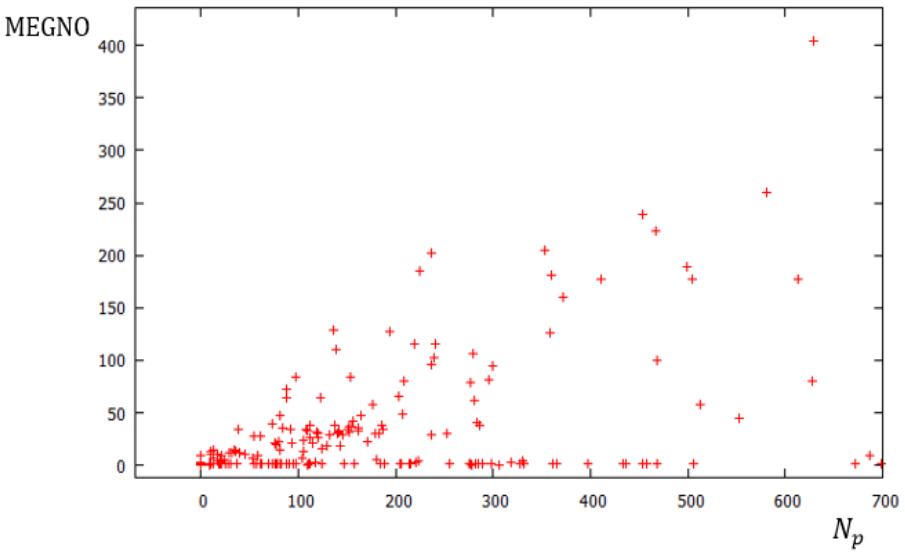

Figure 3.7: Dependence of MEGNO on the number of passages through the unstable regions in case of the superposition of a black hole and the BW/MP ring.

We shall now pass to the superposition with the Morgan-Morgan disc. As we have seen in the Poincaré section 3.3, in this case the geometric criterion even fails to be a necessary condition for chaos to emerge. Motivated by conjecture that this disagreement is due to disc crossings, we check a different correlation: instead of computing the time spent in the unstable regions, we will count how many times the particle passed through the disc located in the equatorial plane. This correlation indeed turned out to work better (such as in the case of figure 3.3 where the geometric criterion predicts completely regular dynamics), but neither it can predict the onset of chaos reliably. For instance in figure 3.8 almost all geodesics pass through the disc, but the Poincaré section is still mostly filled with the "regular" tori intersections.

In the map 3.8 (a) we can see a very small blue unstable region which the geodesics almost never enter. Nevertheless, there is a chaotic orbit near the boundary of the allowed region with the reached value of MEGNO equal to 31.11, thus neither the geometric criterion nor the disc-passage counts is successful.

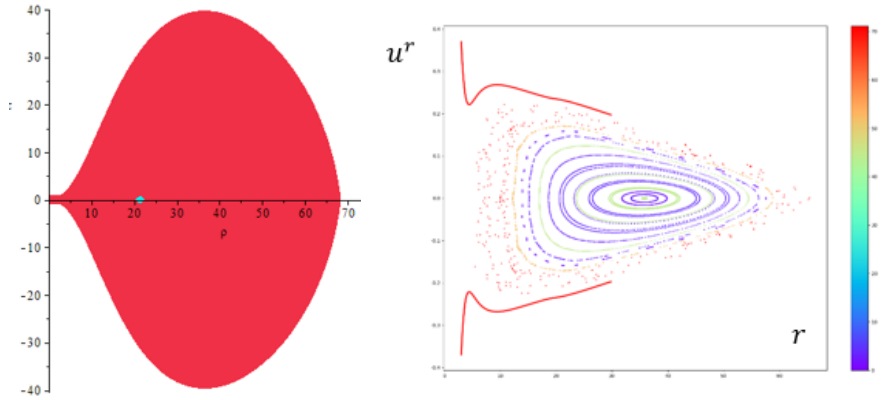

(a) (b)

Figure 3.8: Map of unstable regions (a) and Poincaré section (b) for the superposition of the Schwarzschild black hole and the first inverted MM disc ($m = 0.5M$,$b = 19.493M$, $E = 0.98$, $L_z = 3.75M$).

The summary of the results for the Morgan-Morgan disc is depicted in figure 3.9 where the two different methods are compared while the data from the series in figure 3.8 are not included. Thus despite the failure in the case of the figure 3.8 (b) the counting of the number of disc crossings N_{disc} predicts the appearance of chaos better than the geometric criterion.

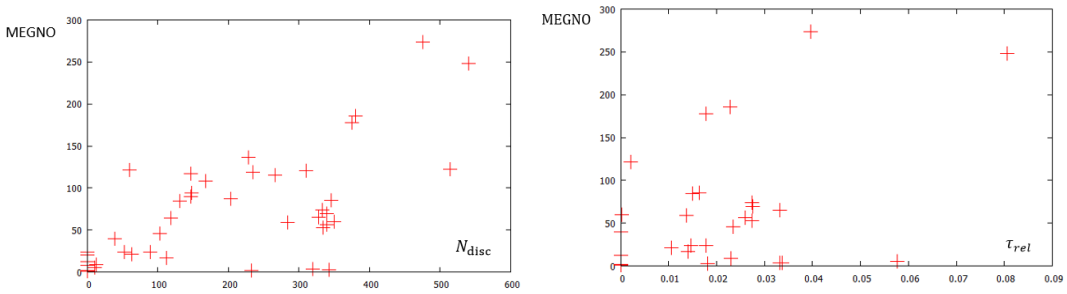

(a) (b)

Figure 3.9: The dependence of MEGNO on the number of crossings through the disc (a) and on the relative time spent in unstable regions (b).

Thus the final statement about our numerical results is that for the superposition of a black hole and a ring the geometric criterion is a necessary condition for the onset of chaos while for the superposition with the inverted Morgan-Morgan disc the criterion fails when the particles are crossing the disc.

It is important to point out that even the chaotic geodesics mostly spend only about one to five percent of proper time in the unstable regions, which is a surprisingly small fraction. To uncover more information, one would have to solve the variational equations to see how the deviation vector behaves inside the unstable region and after leaving it. This would enable us to find a difference between chaotic geodesics and the regular orbits which repeatedly pass through the unstable regions.

The most disproving result for the geometric criterion would be the case of an allowed region completely covered by the unstable region , yet still with regular

dynamics. Such a case I have not encountered. On the contrary, the results seen in figures 3.1 (b) and 3.2 (j) are in accordance with the prediction of the method. The basic idea behind the criterion, the local influence of the unstable regions, is best supported by the orbit in figure 3.5.

Let us add that there are several versions of the geometric criterion. Some of them use the curvature eigenvalues, while others perform some averaging over velocities leading to a quantity proportional to the scalar curvature (this cannot be used in our systems since it is identically zero).

Recently the criterion has been mostly applied in classical mechanics where the motion takes place in an effective manifold (see for example Saa [2004] or Stránský and Cejnar [2015]) Only few articles deal with relativistic systems like the aforementioned Sota et al. [1996].

Overall, most of the authors question the viability of the geometric criteria, often showing numerous counterexamples. At the same time, it is known that there is a connection between curvature of the configuration manifold and chaos (see Ramasubramanian and Sriram [2001]). The results of this thesis support such conclusions. These results do not exclude the possibility that a reliable (analytical) chaos criterion can be found in the future at least for a certain type of dynamical systems.

4. Melnikov's method

In this chapter I will apply the Melnikov method to our perturbed black-hole system and after that I will confront the analytical results of the method with numerical simulations. The application of the method to our system is not as straightforward as it is in most articles concerning Melnikov's method. But before the computation itself we first summarize the (classical) Melnikov method.

4.1 Classical formulation of Melnikov's method

Melnikov's method is an analytical perturbative technique used to detect transverse homoclinic orbits. The method is based on measuring the distance between stable and unstable manifolds of a hyperbolic fixed point. The distance is proportional to the so called Melnikov function (or Melnikov integral) which can be evaluated without solving the equations of motion of the full perturbed system. The potential existence of transverse homoclinic points leads directly (via the Smale-Birkhoff theorem) to the horseshoe-like dynamics which is chaotic (see chapter 1). A detailed discussion of the Melnikov theory may be found in Wiggins [2000].

We start by making some assumptions on our system which will be similar to those in section 1.4., but here we first have to separate the integrable part described by the hamiltonian H_0 and a perturbation by H_1 (neither of these two parts have to be hamiltonian but in our case they will be).

So consider a one-degree-of-freedom system with hamiltonian in the form

$$H(q,p,t,\varepsilon) = H_0(q,p) + \varepsilon H_1(q,p,t) + \mathcal{O}(\varepsilon^2), \tag{4.1}$$

where $\varepsilon > 0$ is a fixed parameter sufficiently small. The hamiltonians H_0 and H_1 may for example be obtained by linearisation of H in ε. The phase space is then three-dimensional and we assume that H_1 is a periodic function of time with period T and that the total hamiltonian H is at least a C^2 function. Denoting $x := (q,p)$, we further assume:

1. H_0 possesses a hyperbolic fixed point P_0 connected to itself by a homoclinic orbit $x_0(t) = (q_0(t), p_0(t))$, $\lim_{t\to\pm\infty} x_0(t) = P_0$.

2. The interior of the homoclinic orbit $\Gamma_{P_0} = W^s(P_0) \cap W^u(P_0) \cup \{p_0\}$ is filled with a continuous family of periodic orbits $x_\alpha(t)$ with period T_α, where $\alpha \in (-1,0)$, $\lim_{\alpha\to 0} x_\alpha(t) = x_0(t)$ and $\lim_{\alpha\to 0} T_\alpha = \infty$.

As we can see for the unperturbed system described by an autonomous hamiltonian H_0, the stable and unstable manifolds coincide along a certain orbit:

$$W^s(P_0) = W^u(P_0) = \{x_0(t), t \in \mathbb{R}\}.$$

This orbit $x_0(t)$ which leaves the fixed point P_0 at $t = -\infty$ and arrives to P_0 at $t = \infty$ is called degenerate homoclinic orbit (sometimes also homoclinic connection or separatrix). The two-dimensional phase space of the unperturbed hamiltonian H_0 is depicted in figure 4.1.

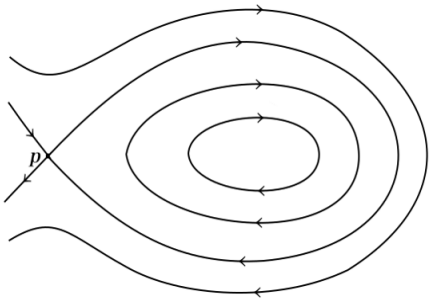

Figure 4.1: A degenerate homoclinic orbit surrounding an area filled with period orbits (from Asano et al. [2016]).

The degenerate homoclinic orbit $x_0(t)$ plays a central role in the Melnikov theory since it is the integration path along which we shall integrate and, therefore, it is necessary to find $x_0(t)$ in a closed form, i.e. expressed using elementary functions. Another important remark is that both the asymptotic manifolds coincide at the degenerate homoclinic orbit and so there is no transverse intersection and therefore no chaotic horseshoe-like dynamics in the unperturbed system.

In order to get chaotic dynamics, the homoclinic tangle needs to be formed. This may happen after the system is perturbed. If the perturbation is sufficiently small for some $\varepsilon > 0$ then the unstable periodic orbit is preserved ($\gamma(t) \to \gamma_\varepsilon(t)$) as are its stable and unstable manifolds which however no longer coincide. The separatrix is broken but we do not know yet if there are some transverse intersections of $W^s_\varepsilon(\gamma_\varepsilon(t))$ and $W^u_\varepsilon(\gamma_\varepsilon(t))$. To verify whether transverse intersections occur we need to measure distance between the two manifolds along the unperturbed homoclinic orbit, which is the idea of the Melnikov method.

A point in the full three-dimensional phase space can be described by a set of three coordinates $(x, \phi(t))$, $x = (q, p)$, where $\phi \in (0, 2\pi)$ and $\phi(t) = \omega t + \phi_0$. The unperturbed periodic orbit then may be parametrized as $\gamma(t) = (P_0, \phi(t)) = (P_0, \omega t + \phi_0)$ and the degenerate homoclinic orbit, now two-dimenional homoclinic manifold, is parametrized as $\Gamma_\gamma(t_0, \phi_0) = (x_0(-t_0), \phi_0)$ (figure 4.2).

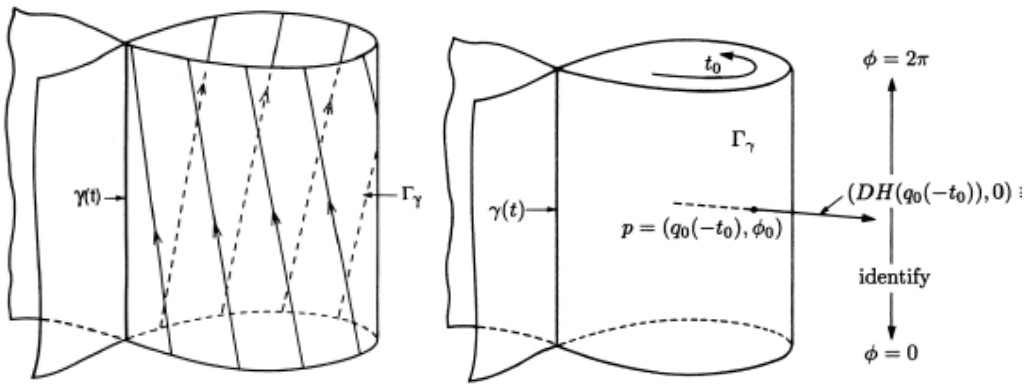

(a) (b)

Figure 4.2: Parametrization of the unperturbed homoclinic manifold Γ_γ (a) and normal vector to Γ_γ (b). Reproduced from Wiggins [2000].

We can define normal vector to Γ_γ at any point using the fact that Γ_γ is a

surface of constant energy ($H_0 = \text{constant}$) (figure 4.2):

$$\pi = \left(\frac{\partial H_0}{\partial q}(x_0(-t_0)), \frac{\partial H_0}{\partial p}(x_0(-t_0)), 0 \right) = (\mathrm{D}H_0(x_0(-t_0)), 0). \tag{4.2}$$

As in chapter 1 we can make a surface of section for some fixed value of ϕ_0 getting the discrete dynamics (figure 4.3). We can now finally define the distance between two points $(x^s_\varepsilon, \phi_0) \in W^s_\varepsilon$ and $(x^u_\varepsilon, \phi_0) \in W^u_\varepsilon$ measured along the unperturbed homoclinic manifold Γ_γ (see figure 4.3),

$$d(t_0, \phi_0, \varepsilon) = \frac{\mathrm{D}H_0(x_0(-t_0)) \cdot (x^s_\varepsilon - x^u_\varepsilon)}{\|\mathrm{D}H_0(x_0(-t_0))\|}. \tag{4.3}$$

It has the form of scalar product whose sign depends on the mutual orientation of the asymptotic manifolds.

The points $(x^s_\varepsilon, \phi_0)$ and $(x^u_\varepsilon, \phi_0)$ lie on the intersection of the straight line defined by the normal vector with the respective manifold. However, the intersection with W^s_ε (W^u_ε) may not be unique, in fact there can be infinitely many of them for some given point of Γ_γ (figure 4.3 (b)), but the points $(x^s_\varepsilon, \phi_0)$ and $(x^u_\varepsilon, \phi_0)$ are defined uniquely. The point $(x^s_\varepsilon, \phi_0) \in \pi \cap W^s_\varepsilon(\gamma_\varepsilon(t))$ is the closest to $\gamma_\varepsilon(t)$ in terms of positive time of flight on $W^s_\varepsilon(\gamma_\varepsilon(t))$, i.e., for all $t > 0$, $(x^s_\varepsilon(t), \phi(t)) \cap \pi = \emptyset$ and $(x^s_\varepsilon(0), \phi(0)) = (x^s_\varepsilon, \phi_0)$. The point lying on the unstable manifold is defined in the same way, just with the opposite direction of time evolution.

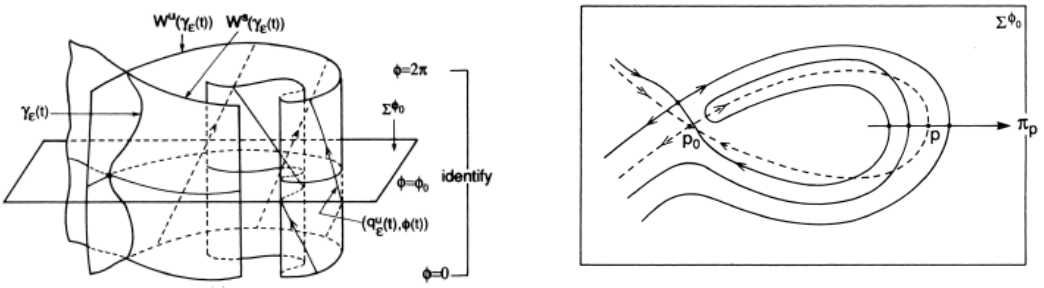

(a) (b)

Figure 4.3: Projection of the asymptotic manifolds on a surface of section (from Wiggins [2000]).

We can now measure the distance $d(t_0, \phi_0, \varepsilon)$ for every $t_0 \in \mathbb{R}, \phi_0 \in (0, 2\pi)$, but, as we can see, to compute the distance, the knowledge of x^s_ε and x^u_ε is required which is equivalent to the knowledge of the full (perturbed) dynamics. Nevertheless, we will assume the perturbation is sufficiently small to permit the Taylor expansion of $d(t_0, \phi_0, \varepsilon)$, which leads to an easily computable quantity called Melnikov's function (or integral). In the first order we have:

$$d(t_0, \phi_0, \varepsilon) = d(t_0, \phi_0, 0) + \varepsilon \frac{\partial d}{\partial \varepsilon}(t_0, \phi_0, 0) + \mathcal{O}(\varepsilon^2), \tag{4.4}$$

where the zero-order term drops out since the unperturbed asymptotic manifolds coincide, so we are left with

$$d(t_0, \phi_0, \varepsilon) = \varepsilon \frac{M(t_0, \phi_0)}{\|\mathrm{D}H_0(x_0(-t_0))\|} + \mathcal{O}(\varepsilon^2), \tag{4.5}$$

where the function $M(t_0, \phi_0)$ is the Melnikov function defined as

$$M(t_0, \phi_0) = \mathrm{D}H_0(x_0(-t_0)) \cdot \left(\frac{\partial x^s_\varepsilon}{\partial \varepsilon} - \frac{\partial x^u_\varepsilon}{\partial \varepsilon} \right). \tag{4.6}$$

From (4.6) we can immediately see that for ε sufficiently small: $d(t_0, \phi_0, \varepsilon) = 0 \Leftrightarrow M(t_0, \phi_0) = 0$. Thus finding the intersections of the asymptotic manifolds is equivalent to finding zeros of the function $M(t_0, \phi_0)$.

Performing several "clever" manipulations (see Wiggins [2000]), one can express the Melnikov function in the form of an integral,

$$M(t_0, \phi_0) = \int_{-\infty}^{\infty} \{H_0, H_1\}(x_0(t), \omega t + \omega t_0 + \phi_0) \mathrm{d}t. \tag{4.7}$$

From this form one can deduce that varying t_0 is equivalent to changing ϕ_0, so we can simply replace $\omega t_0 + \phi_0 \to t_0$ and the Melnikov function is then a function of just one variable,

$$M(t_0) = \int_{-\infty}^{\infty} \{H_0, H_1\}(x_0(t), t + t_0) \mathrm{d}t. \tag{4.8}$$

This is an integral of the Poisson bracket of H_0 with H_1 along the unperturbed homoclinic orbit. The Melnikov function is obviously periodic, with the same period T as H_1: $M(t_0 + T) = M(t_0)$.

The connection between the Melnikov function and the existence of transverse homoclinic points can be stated in the following theorem:

Theorem 4.1.1. *Suppose there exists $\bar{t_0} \in \langle 0, T \rangle$ such that*

1. $M(\bar{t_0}) = 0$,
2. $\dfrac{\mathrm{d}M}{\mathrm{d}t_0}(\bar{t_0}) \neq 0$.

Then for $\varepsilon > 0$ sufficiently small $W^s_\varepsilon(\gamma_\varepsilon(t))$ and $W^u_\varepsilon(\gamma_\varepsilon(t))$ intersect transversally. Moreover, if $M(\bar{t_0}) \neq 0$ for all $\bar{t_0} \in \langle 0, T \rangle$, then $W^s_\varepsilon(\gamma_\varepsilon(t)) \cap W^u_\varepsilon(\gamma_\varepsilon(t)) = \emptyset$.

While the first condition in 4.1.1 obviously means that the asymptotic manifolds intersect, the second one ($\dfrac{\mathrm{d}M}{\mathrm{d}t_0}(\bar{t_0}) \neq 0$) is equivalent to the transversality of the intersection. Together both conditions can be summarized as "$M(t_0)$ has simple zeros". The second condition is thus necessary; one of the situations when it does not hold is the case when $M(t_0) = 0$ identically, which means that the degenerate homoclinic orbit is preserved under the given perturbation.

Therefore, to apply the Melnikov method, we first need to solve the unperturbed equations of motion in order to find the degenerate homoclinic orbit $x_0(t)$, and after that we compute the Poisson bracket between the two hamiltonians and evaluate the Melnikov function $M(t_0)$. If $M(t_0)$ has simple zeros, then W^s and W^u intersect transversally and we can conclude that the dynamics close to the original separatrix is chaotic. If there are no simple zeroes, then the homoclinic chaos does not occur.

However, we will see it is not straightforward to apply the method to our system of a black hole perturbed by an additional source.

4.2 Pseudo-Newtonian versus relativistic approach

In the second chapter we have seen that while the first metric function ν superposes linearly the second one (λ) does not (see equations (2.2) and (2.3)). It is actually difficult to find λ for the superposition of a Schwarzschild black hole and a ring or a disc. That is the reason why I decided to apply the method to the pseudo-Newtonian system first. On the other hand, for the superposition of the extreme Reissner-Nordström black hole and the Majumdar-Papapetrou ring we can follow a fully relativistic treatment.

In the pseudo-Newtonian hamiltonian the Schwarzschild black hole will be approximated by the Nowak-Wagoner potential V_{NW} (2.8), and the potential of the ring or disc will simply be given by the first metric function which we denote as ν_1. The pseudo-Newtonian hamiltonian describing a particle of mass m_0 then takes the form

$$H(r,\theta,p_r,p_\theta,p_\phi) = \frac{p^2}{2m_0} + m_0 V_{NW}(r) + m_0\nu_1(r,\theta), \tag{4.9}$$

where $\frac{p^2}{2m_0}$ is the classical kinetic term. To apply the Melnikov method we first need to separate the perturbation from the fully integrable unperturbed part of H, i.e. to write

$$H(r,\theta,p_r,p_\theta,p_\phi) = H_0(r,\theta,p_r,p_\theta,p_\phi) + mH_1(r,\theta), \tag{4.10}$$

where the unperturbed hamiltonian H_0 reads

$$H_0(r,\theta,p_r,p_\theta,p_\phi) = \frac{1}{2m_0}\left[p_r^2 + \frac{1}{r^2}\left(p_\theta^2 + \frac{p_\phi^2}{\sin^2\theta}\right)\right] + m_0 V_{NW}(r) \tag{4.11}$$

and the perturbation hamiltonian is

$$H_1(r,\theta) = \frac{m_0}{m}\nu_1(r,\theta). \tag{4.12}$$

The small perturbation parameter ε is in our hamiltonian the mass of a ring or a disc m which we assume to be sufficiently small relative to the black-hole mass M. The metric function ν_1 is actually proportional to the ring/disc mass and so the perturbation hamiltonian H_1 does not depend on m.

We have chosen the Nowak-Wagoner potential, because it is the only pseudo-Newtonian potential for which I was able to find the explicit form of the homoclinic orbit.

To conclude the part on pseudo-Newtonian approach, we would like to make an important remark regarding coordinates. The functions ν_1 are given in the Weyl coordinates (see chapter 2) and so they need to be transformed into spherical-like coordinates and for this purpose we use the relativistic transformation relation (2.6) even though we now work effectively in the Euclidean space.

The relativistic version of our problem is slightly more difficult. As already mentioned in chapter 2, the hamiltonian is described by expression (2.20) that

we need to linearize in the ring/disc mass to get the hamiltonian separated to H_0 and H_1. The Taylor expansion of (2.20) gives

$$\begin{aligned} H &= \frac{1}{2m_0}\Big(g^{\mu\nu}(m=0) + m\frac{\partial g^{\mu\nu}(m=0)}{\partial m} + \mathcal{O}(m^2)\Big)p_\mu p_\nu = \\ &= \frac{1}{2m_0}g^{(0)\mu\nu}p_\mu p_\nu + m\frac{1}{2m_0}g^{(1)\mu\nu}p_\mu p_\nu + \mathcal{O}(m^2) = \\ &= H_0(r,\theta,p_t,p_r,p_\theta,p_\phi) + mH_1(r,\theta,p_t,p_r,p_\theta,p_\phi) + \mathcal{O}(m^2). \end{aligned} \tag{4.13}$$

The first-order term in the expansion of the contravariant metric tensor can also be expressed using the covariant metric. Assuming that our (Weyl) metric is diagonal, we have

$$g^{\mu\nu} = \frac{1}{g^{(0)}_{\mu\nu}} + m\frac{-g^{(1)}_{\mu\nu}}{(g^{(0)}_{\mu\nu})^2} + \mathcal{O}(m^2). \tag{4.14}$$

This form of expansion will be used in the following sections.

The unperturbed hamiltonian H_0 describes the black hole itself. For the Schwarzschild black hole (2.5) we get

$$H_0 = \frac{1}{2m_0}\Big[-\frac{1}{1-\frac{2M}{r}}p_t^2 + \Big(1-\frac{2M}{r}\Big)p_r^2 + \frac{1}{r^2}\Big(p_\theta^2 + \frac{p_\phi^2}{\sin^2\theta}\Big)\Big], \tag{4.15}$$

and similarly for the extreme Reissner-Nordström black hole (2.15)

$$H_0 = \frac{1}{2m_0}\Big[-\frac{1}{\big(1-\frac{M}{r}\big)^2}p_t^2 + \Big(1-\frac{M}{r}\Big)^2 p_r^2 + \frac{1}{r^2}\Big(p_\theta^2 + \frac{p_\phi^2}{\sin^2\theta}\Big)\Big]. \tag{4.16}$$

We thus have all the hamiltonians necessary for computing the Melnikov function, but before we can do that we first need to reformulate the Melnikov method as well as transform the canonical coordinate in our hamiltonians.

4.3 Modification of Melnikov's method

Comparing the hamiltonians (4.10) and (4.13) with the assumed form of hamiltonian (4.1) required for the Melnikov method, we immediately see that they differ considerably. First there is no time dependence in our perturbations which describe static discs/rings. And second, we have way too many degrees of freedom in our system while (4.1) is only a one-degree-of-freedom hamiltonian.

Solution to these problems can be found in Holmes and Marsden [1983] where the authors considered a hamiltonian in the form

$$H(q,p,\psi,J) = H_0(q,p,J) + \varepsilon H_1(q,p,\psi,J) + \mathcal{O}(\varepsilon^2). \tag{4.17}$$

This does not explicitly depend on time and describes a two-degree-of-freedom system. The idea behind the reformulation of the Melnikov method lies in the replacement of time by another coordinate $\psi \in (0, 2\pi)$ which is periodic while

the role of the hamiltonian will now be played by its conjugated momentum J. As in the original formulation, we assume that H_0 possesses a hyperbolic fixed point P_0 in the reduced phase space described by $x = (q, p)$ and a degenerate homoclinic orbit $(x_0(t))$ connected to the fixed point ($\lim_{t\to\pm\infty} x_0(t) = P_0$) for some fixed value of J. The relation between ψ and time t in the unperturbed system is from the Hamilton equations,

$$\dot{\psi} = \Omega(x, J) = \frac{\partial H_0}{\partial J}(x, J). \tag{4.18}$$

Solving this differential equation allows to parametrize the homoclinic orbit by ψ and subsequently rewrite the evolution in terms of this new variable.

The motion in the perturbed system is confined to the energy hypersurface $H(x, \psi, J) = h$, and this equation has to be invertible in order to express $J = J(x, \psi, h)$ with h fixed. Thus we have a new "hamiltonian" J and the Melnikov function can be rewritten according to Holmes and Marsden [1983]

$$M(\psi_0) = \int_{-\infty}^{\infty} \frac{1}{\Omega(x_0(\psi), J)} \left\{ H_0, \frac{H_1}{\Omega} \right\} (x_0(\psi), \psi + \psi_0, J) \mathrm{d}\psi. \tag{4.19}$$

The Poisson bracket is computed only in the variable x while the momentum J is kept fixed. If the system has only one homoclinic orbit for some value of J, then fixing J is equivalent to fixing the energy surface $h = H_0(x_0(\psi), J)$.

The original theorem (4.1.1) is then modified for the hamiltonian (4.17) (for details see Holmes and Marsden [1983]) into

Theorem 4.3.1. *Consider a hamiltonian in the form* (4.17) *and assume that, for some fixed value of J, $H_0(x, J)$ has a homoclinic orbit connected to a hyperbolic fixed point, and that $\Omega(x_0(\psi), J) > 0$. Then if $M(\psi_0)$ has simple zeros and $\varepsilon > 0$ is sufficiently small, the system* (4.17) *has transverse homoclinic orbits (the asymptotic manifolds intersect transversally) on the energy surface $H = h$, where $h = H_0(x_0(\psi), J)$.*

The important part of this theorem is the statement about the energy surface. By energy we mean any integral of motion of the complete hamiltonian H which in our case is the energy E (p_t) and the z-component of the angular momentum L_z (p_ϕ). So fixing these integrals of motion and a homoclinic orbit (if it exists for some E and L_z) automatically fixes the value of J. It may thus happen that for some values of E and L_z there is no homoclinic orbit and therefore no homoclinic chaos in the perturbed system.

Getting back to the perturbed black hole, we know that due to the existence of two integrals of motion E and L_z we reduced our system to two degrees of freedom with coordinates (r, θ). In the (r, p_r) subspace, we have the homoclinic orbit (x in (4.17)) but the angular coordinate θ cannot play the role of ψ since its conjugate momentum p_θ is not an integral of motion in the unperturbed system (H_0 depends on θ).

In order to have the hamiltonians in the form (4.17), we need to pass to a new set of coordinates on the phase space, i.e. to perform a canonical transformation:

$$(\theta, p_\theta) \to (\vartheta, J_\vartheta).$$

As we have said, it is necessary for J_ϑ to be an integral of motion and this can be satisfied if J_ϑ is an action variable (see chapter 1). By comparing our pseudo-Newtonian and relativistic hamiltonians, (4.13), (4.15) and (4.16), we can see that they include a common part containing the variable θ,

$$L^2 := p_\theta^2 + \frac{p_\phi^2}{\sin^2\theta}. \tag{4.20}$$

Denoting this structure by L^2 is natural since it can be interpreted as a square of the total angular momentum. The variable L is an integral of motion and this allows to compute the action variable J_ϑ using the definition (1.10)

$$J_\vartheta = \frac{1}{2\pi}\oint p_\theta \,\mathrm{d}\theta = \frac{1}{2\pi}\int_{\theta_{\min}}^{\theta_{\max}} \sqrt{L^2 - \frac{p_\phi^2}{\sin^2\theta}}\,\mathrm{d}\theta + \frac{1}{2\pi}\int_{\theta_{\max}}^{\theta_{\min}} -\sqrt{L^2 - \frac{p_\phi^2}{\sin^2\theta}}\,\mathrm{d}\theta. \tag{4.21}$$

The integral is taken over the whole period of motion between two turning points which are determined by $p_\theta = 0$. Thus from (4.20) we have $\theta_{\min} = \arcsin\frac{p_\phi}{L}$ and $\theta_{\max} = \pi - \arcsin\frac{p_\phi}{L}$.

From chapter 1 we know that the Hamilton-Jacobi equation of the unperturbed system is separable (equation (1.7)), which implies $p_\theta = \frac{\partial S_\theta}{\partial\theta}$ and allows to compute J_ϑ,

$$J_\vartheta = \frac{1}{\pi}\int_{\theta_{\min}}^{\theta_{\max}} \sqrt{L^2 - \frac{p_\phi^2}{\sin^2\theta}}\,\mathrm{d}\theta = \frac{1}{\pi}\int_{\theta_{\min}}^{\theta_{\max}} \frac{\partial S_\theta}{\partial\theta}(\theta, L, p_\phi)\,\mathrm{d}\theta. \tag{4.22}$$

The primitive function of $\sqrt{L^2 - \frac{p_\phi^2}{\sin^2\theta}}$ reads, up to some constant,

$$\begin{aligned} S_\theta = \tfrac{1}{2}\arctan\left(\frac{L^2\cos\theta + L^2 - {p_\phi}^2}{p_\phi\sqrt{-L^2(\cos\theta)^2 + L^2 - {p_\phi}^2}}\right)p_\phi + \tfrac{1}{2}\arctan\left(\frac{L^2\cos\theta - L^2 + {p_\phi}^2}{p_\phi\sqrt{-L^2(\cos\theta)^2 + L^2 - {p_\phi}^2}}\right)p_\phi - \\ - \arctan\left(\frac{L\cos\theta}{\sqrt{-L^2(\cos\theta)^2 + L^2 - {p_\phi}^2}}\right)L. \end{aligned} \tag{4.23}$$

Taking the limits to the turning points, we get the action variable

$$\begin{aligned} J_\vartheta = \frac{1}{\pi}\lim_{\theta\to\theta_{\max}} S_\theta - \frac{1}{\pi}\lim_{\theta\to\theta_{\min}} S_\theta = \frac{1}{\pi}\Big(-\frac{\pi}{4}p_\phi - \frac{\pi}{4}p_\phi + \frac{\pi}{2}L\Big) - \\ - \frac{1}{\pi}\Big(\frac{\pi}{4}p_\phi + \frac{\pi}{4}p_\phi - \frac{\pi}{2}L\Big) = L - p_\phi \end{aligned}. \tag{4.24}$$

We can see that it is indeed an integral of motion. To find its conjugated coordinate ϑ, we can use the transformation equation (1.5b),

$$\vartheta = \frac{\partial S_\theta}{\partial J_\vartheta}(\theta, p_\phi, J_\vartheta) = \frac{\partial S_\theta}{\partial L}(\theta, p_\phi, L). \tag{4.25}$$

The only coordinates that we are transforming are θ and p_θ, and that is the reason we do not care about other parts of the generating function S and we can

manage with only S_θ. Inverting equation (4.25), we can express θ as a function of ϑ, and so the final transformation relations are

$$\theta = \pi - \arccos\left(\frac{\tan\vartheta}{L}\sqrt{\frac{L^2 - {p_\phi}^2}{(\tan\vartheta)^2 + 1}}\right), \qquad L = J_\vartheta + p_\phi. \tag{4.26}$$

Having obtained the transformation relations, we can finally express our hamiltonians in terms of these new variables. For example, the unperturbed pseudo-Newtonian hamiltonian now takes the form

$$H_0(r, p_r, J_\vartheta, p_\phi) = \frac{1}{2m_0}\left(p_r^2 + \frac{(J_\vartheta + p_\phi)^2}{r^2}\right) + m_0 V_{NW}(r). \tag{4.27}$$

The result is similar for the relativistic hamiltonians since they also contain the angular- momentum part $\frac{(J_\vartheta + p_\phi)^2}{r^2}$.

So now we have H_0 which does not depend on an angular coordinate while the angular momenta J_ϑ and p_ϕ (L_z) are treated on equal footing. As for the perturbation, the variable θ is replaced by ϑ in H_1 using (4.26). The complete hamiltonian after the transformation then reads

$$H(r, \vartheta, p_r, J_\vartheta) = H_0(r, p_r, J_\vartheta) + mH_1(r, \vartheta, p_r, J_\vartheta) + \mathcal{O}(\varepsilon^2). \tag{4.28}$$

In this formula we ignored the additional momenta p_ϕ and p_t since they are just parameters like the disc/ring radius. Thus we have succeeded in transforming our hamiltonians to the form (4.17), where ϑ plays the role of ψ.

Before passing to another section, I would like to remark that the term $\frac{\partial S}{\partial t}$ in the hamiltonian transformation equation (1.5c) gives only a constant and that is why we have omitted it in (4.27) and (4.28). The other point is that while J_ϑ is an action variable, the pair (ϑ, J_ϑ) does not constitute the action-angle coordinates, because H_0 still depends on r. Nevertheless for our purposes it is important that the Hamilton equations in (ϑ, J_ϑ) are equivalent to those expressed in (θ, p_θ).

4.4 Homoclinic orbits

In order to compute the Melnikov integral we first need to find the integration path which is the (degenerate) homoclinic orbit (separatrix). From now on we will use notation $E := -p_t$, $L_z = p_\phi$, and to eliminate the particle mass m_0 we introduce renormalized quantities $e := \frac{E}{m_0}$, $l := \frac{L}{m_0}$ and so on.

Let us start from the pseudo-Newtonian Schwarzschild black hole described by the Nowak-Wagoner potential. We need to solve the equations of motion to find the orbit which asymptotically approaches the fixed point in both directions of time. We will use the effective-potential method. From the pseudo-Newtonian hamiltonian $H_0 = E$ we get

$$\frac{1}{2}v_r^2 = e - \left[\frac{l^2}{2r^2} - \frac{M}{r}\left(1 - \frac{3M}{r} + \frac{12M^2}{r^2}\right)\right] = e - V_{\text{eff}}(r) \geq 0. \tag{4.29}$$

First thing we need is the location of the unstable circular orbit. We find it by solving the equation $\frac{\mathrm{d}V_{eff}}{\mathrm{d}r}(r) = 0$. The zero point closer to the origin is the hyperbolic fixed point,

$$r_{\mathrm{hyp}} = \frac{6\,M^2 + l^2 - \sqrt{-108\,M^4 + 12\,M^2 l^2 + l^4}}{2M}. \tag{4.30}$$

Energy of the homoclinic orbit is the same as that of the unstable hyperbolic orbit and so $e = V_{\mathrm{eff}}(r_{\mathrm{hyp}})$. The expression for e is rather long and it is useless to present it here. The choice of the energy level is depicted in figure 4.4 and the homoclinic orbit is seen to exist only for some values of l (we will get back to this problem later).

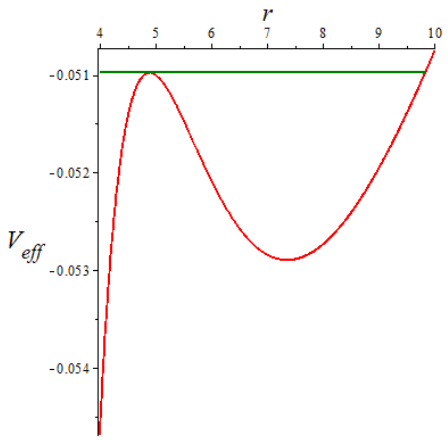

Figure 4.4: NW effective potential (red) and energy level corresponding to the homoclinic orbit (green).

We will proceed by introducing the variable $u := \frac{1}{r}$ and then we will use a common trick by writing

$$v_r = \frac{\mathrm{d}r}{\mathrm{d}t} = \frac{\mathrm{d}u}{\mathrm{d}\vartheta}\frac{\mathrm{d}r}{\mathrm{d}u}\frac{\mathrm{d}\vartheta}{\mathrm{d}t} = \frac{\mathrm{d}u}{\mathrm{d}\vartheta}\left(-\frac{1}{u^2}\right)\frac{l}{r^2} = -l\frac{\mathrm{d}u}{\mathrm{d}\vartheta}, \tag{4.31}$$

which puts the equation of motion (4.29) into the form

$$\left(\frac{\mathrm{d}u}{\mathrm{d}\vartheta}\right)^2 = 2\,\frac{e}{l^2} - u^2 + 2\,\frac{Mu\,(12\,M^2u^2 - 3\,Mu + 1)}{l^2}. \tag{4.32}$$

This can be further simplified using the product form of the right-hand side,

$$\left(\frac{\mathrm{d}u}{\mathrm{d}\vartheta}(\vartheta)\right)^2 = k(u(\vartheta) - u_{\mathrm{hyp}})^2(u(\vartheta) - u_{\mathrm{max}}) \tag{4.33}$$

where $u_{\mathrm{hyp}} = \frac{1}{r_{\mathrm{hyp}}}$, $u_{\mathrm{max}} = \frac{1}{r_{\mathrm{max}}}$ and r_{max} corresponds to the maximal radius the particle can reach (i.e. the turning point). Like the energy, the quantities k and u_{max} are some functions of M and l which we do not show here since the expressions are too long.

Equation (4.33) can be solved in a closed form

$$u(\vartheta) = (u_{\mathrm{hyp}} - u_{\mathrm{max}})\tanh^2\left(\frac{1}{2}\sqrt{k(u_{\mathrm{hyp}} - u_{\mathrm{max}})}\vartheta\right) + u_{\mathrm{max}}. \tag{4.34}$$

The homoclinic orbit is parametrized so that $u(0) = u_{\max}$ (the turning point) and $u(\vartheta \to \pm\infty) = u_{\text{hyp}}$ which are the properties we would expect from a homoclinic orbit. The homoclinic orbit is depicted in figure 4.5 where we can see how it looks like in the equatorial plane of the configuration space. The motion is planar and can be described using polar coordinates $r = \frac{1}{u}$ and $\phi = \vartheta$.

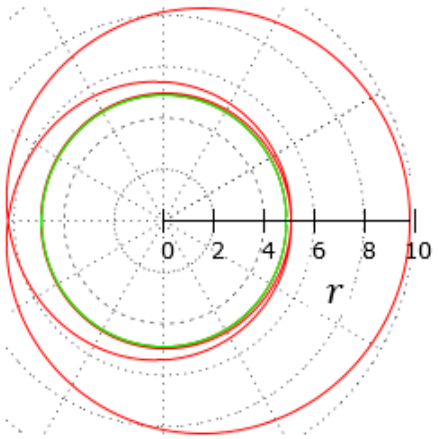

Figure 4.5: A polar graph of the homoclinic orbit (4.34) of the NW potential (red), also showing the unstable circular orbit (green).

Now we turn to the relativistic case. For the Schwarzschild black hole the result surprisingly has the same form as (4.34) but with different coefficients. The coefficients even have simpler form than those of the pseudo-Newtonian black hole and so we can write them down here:

$$u_{\text{hyp}} = \frac{l + \sqrt{-12\,M^2 + l^2}}{6Ml}, \quad u_{\max} = \frac{l - 2\sqrt{-12M^2 + l^2}}{6Ml}, \quad k = 2M. \tag{4.35}$$

This result had already been obtained by Bombelli and Calzetta [1992] but we recomputed it with our result differing from theirs by rescaling the variable u by the factor of $2M$. So we see that in this feature the Nowak-Wagoner potential represents the black hole reasonably even though the coefficients differ.

We shall now proceed to the extreme Reissner-Nordström black hole, discussing the computation in more details than in the Schwarzschild case. To obtain the effective-potential equation we will use the hamiltonian (4.16). Using again the trick (4.31) (with replacement $t \to \tau$) and the fact that along a geodesic $H_0 = -\frac{1}{2}m_0$, we have

$$\left(\frac{\mathrm{d}u}{\mathrm{d}\vartheta}\right)^2 = \frac{e^2 - (1 - Mu)^2\,(l^2u^2 + 1)}{l^2}, \tag{4.36}$$

where again $u = \frac{1}{r}$. In contrast to the Schwarzschild black hole, the right-hand side is a polynomial of the fourth order which has three stationary points (figure 4.6): one is the usual stable circular orbit, another one is the searched unstable periodic orbit. The third stationary point of the effective potential is located at the horizon $r = M$ with $V_{\text{eff}}(r = M) = 0$ and it is a minimum. The stable circular orbit on the horizon would necessarily have $p_t = 0$, which due to the

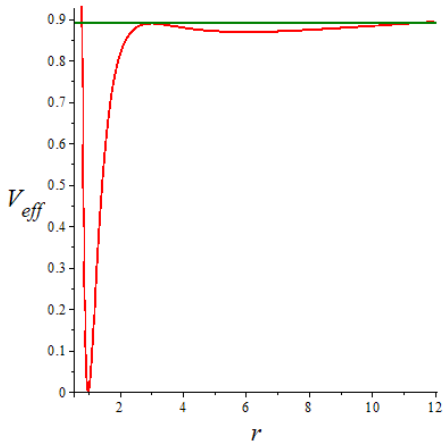

Figure 4.6: Effective potential of the extreme Reissner-Nordström black hole (red) and the energy level corresponding to the homoclinic orbit (green).

four-momentum normalization implies $p_i = 0$. So the circular orbit on $r = M$ could be interpreted as that of an infinitely redshifted photon.

As in the previous case we, we fix the energy by $e = V_{\text{eff}}(r_{\text{hyp}})$ and rewrite the equation (4.36) as

$$\left(\frac{\mathrm{d}u}{\mathrm{d}\vartheta}(\vartheta)\right)^2 = -M^2(u(\vartheta) - u_{\text{hyp}})^2(u(\vartheta) - u_{\text{max}})(u(\vartheta) - u_{\text{in}}), \tag{4.37}$$

where u_{in} is the turning point located inside the black hole (see figure 4.6). Hence we conclude that our homoclinic orbit is located in the interval $u \in (u_{\text{max}}, u_{\text{hyp}})$, or equivalently $r \in (r_{\text{hyp}}, r_{\text{max}})$. Due to the inequality $u_{\text{max}} \leq u \leq u_{\text{hyp}}$, the minus sign in front of M^2 is cancelled and thus equation (4.37) holds without any seeming inconsistency. Expressions for the turning points are still quite simple,

$$u_{\text{hyp}} = \frac{l + \sqrt{-8\,M^2 + l^2}}{4Ml} \tag{4.38}$$

and

$$u_{\text{max/in}} = \frac{\frac{3}{4}\,l - \frac{1}{4}\sqrt{-8\,M^2 + l^2} \mp \frac{1}{2}\sqrt{l^2 + \sqrt{-8\,M^2 + l^2}\,l}}{lM}. \tag{4.39}$$

Finally, solving the equation (4.37) with the condition that u_{max} is the turning point of the homoclinic orbit, we have

$$u(\vartheta) = u_{\text{hyp}} + \frac{2\beta}{u_{\text{in}} + u_{\text{max}} - 2\,u_{\text{hyp}} + (u_{\text{in}} - u_{\text{max}})\cosh\left(\sqrt{-M^2\beta}\vartheta\right)} \tag{4.40}$$

where $\beta = (u_{\text{in}} - u_{\text{hyp}})\,(u_{\text{max}} - u_{\text{hyp}})$. This is the (degenerate) homoclinic orbit of the extreme Reissner-Nordström black hole. We can again see that $u(\vartheta \to \pm\infty) = u_{\text{hyp}}$. The spatial representation (polar graph) of the homoclinic orbit is depicted in figure 4.7.

Thus we have all the necessary ingredients prepared to compute the Melnikov function.

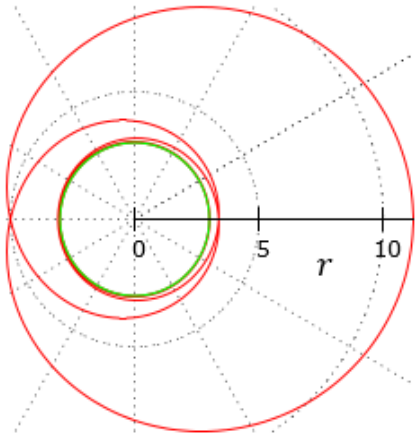

Figure 4.7: The homoclinic orbit of the extreme Reissner-Nordström black hole in the physical space (red) with the unstable circular orbit shown (green).

4.5 Calculation of the Melnikov function

To evaluate the Melnikov function, we first need to compute the Poisson brackets in variables (r, p_r) which are part of the modified definition of the Melnikov function (4.19). Another necessary component is the unperturbed angular frequency Ω which has the same form in the pseudo-Newtonian and in the relativistic case:

$$\Omega(r, J) = \frac{\partial H_0}{\partial J_\vartheta} = \frac{1}{m_0}\frac{J_\vartheta + L_z}{r^2} = \frac{l}{r^2}. \tag{4.41}$$

For simplicity of notation, we will from now on work with $l = \frac{1}{m_0}(J_\vartheta + L_z)$ instead of J_ϑ. We will first find the Melnikov function for the pseudo-Newtonian hamiltonian (4.10) whose unperturbed part is given by (4.11) and $H_1 = \frac{m_0}{m}\nu_1$. The function ν_1 has to be transformed to the spherical coordinates using (2.6). The Poisson brackets are then

$$\left\{H_0, \frac{H_1}{\Omega}\right\} = \frac{\partial H_0}{\partial r}\frac{\partial}{\partial p_r}\left(\frac{H_1}{\Omega}\right) - \frac{\partial H_0}{\partial p_r}\frac{\partial}{\partial r}\left(\frac{H_1}{\Omega}\right) = -\frac{p_r}{m_0}\left(\frac{r^2}{l}\frac{\partial H_1}{\partial r} + 2H_1\frac{r}{l}\right) \tag{4.42}$$

and thus the complete integrand reads

$$\frac{1}{\Omega}\left\{H_0, \frac{H_1}{\Omega}\right\} = -v_r\frac{r^3}{l^2}\left(2H_1 + r\frac{\partial H_1}{\partial r}\right). \tag{4.43}$$

Performing the canonical transformation:

$$H_1(r, \theta) \to H_1(r, \vartheta, L, L_z)$$

which we derived in previous sections (see equation (4.26)), inserting the homoclinic orbit $(r(\vartheta), v_r(\vartheta))$ into (4.43) and integrating along the homoclinic orbit gives us the pseudo-Newtonian Melnikov function,

$$M(\vartheta_0) = \int_{-\infty}^{\infty}(-v_r(\vartheta))\frac{r^3(\vartheta)}{l^2}\left[2H_1(r(\vartheta), \vartheta+\vartheta_0)+r(\vartheta)\frac{\partial H_1}{\partial r}(r(\vartheta), \vartheta+\vartheta_0)\right]\mathrm{d}\vartheta, \tag{4.44}$$

where the relation between the homoclinic orbit $u(\vartheta)$ we computed (equation (4.34)) and $(r(\vartheta), v_r(\vartheta))$ is obviously

$$r(\vartheta) = \frac{1}{u(\vartheta)}, \qquad v_r(\vartheta) = -l\frac{\mathrm{d}u(\vartheta)}{\mathrm{d}\vartheta}.$$

The resulting Melnikov function $M(\vartheta_0)$ is expressed with the explicit dependences of the integrand on variables ϑ and ϑ_0, but the dependence on the fixed parameters l and l_z is omitted for brevity.

In the pseudo-Newtonian description, H_1 represents either the inverted MM disc (2.10) or the BW ring (2.11) surrounding the Schwarzschild black hole. We shall now continue with the relativistic Melnikov function whose derivation is slightly more complicated.

Our relativistic perturbation hamiltonian H_1 is given by (4.13) and (4.14),

$$H_1 = \frac{1}{2m_0}\left[-\frac{g^{(1)}_{tt}}{(g^{(0)}_{tt})^2}E^2 - \frac{g^{(1)}_{rr}}{(g^{(0)}_{rr})^2}p_r^2 - \frac{g^{(1)}_{\theta\theta}}{(g^{(0)}_{\theta\theta})^2}\left(L^2 - \frac{L_z^2}{\sin^2\theta}\right)^2 - \frac{g^{(1)}_{\phi\phi}}{(g^{(0)}_{\phi\phi})^2}L_z^2\right], \quad (4.45)$$

where we have already eliminated p_θ using (4.20). The metric also has to be transformed to the spherical-like coordinates according to the relation (2.6) or (2.16) (for the Reissner-Nordström black hole and MP ring). And before computing the Poisson brackets we perform the canonical transformation $\theta = \theta(\vartheta, L, L_z)$ (relation (4.26)).

Recalling the original definition of the Melnikov function (equation (4.5)), we see that it is a part of the linear term in the expansion of the distance between the asymptotic manifolds, or, in other words, we measure the distance in the $\mathcal{O}(m)$ approximation. Consequently inside the Melnikov function we raise and lower indices using only the unperturbed metric, for example

$$p_r = g^{(0)}_{rr}p^r + \mathcal{O}(m).$$

The term containing $g^{(1)}_{rr}$ would then contribute to the distance expansion as $\mathcal{O}(m^2)$ and thus we neglect it there.

The Poisson brackets taken in (r, p_r) are

$$\begin{aligned}\left\{H_0, \frac{H_1}{\Omega}\right\} &= \frac{\partial H_0}{\partial r}\frac{1}{\Omega}g^{(1)rr}\frac{p_r}{m_0} - g^{(0)rr}\frac{p_r}{m_0}\left(\frac{1}{\Omega}\frac{\partial H_1}{\partial r} + \frac{2r}{l}H_1\right) = \\ &= u^r\left[\frac{\partial H_0}{\partial r}\frac{r^2}{l}\left(\frac{-g^{(1)}_{rr}}{g^{(0)}_{rr}}\right) - \left(\frac{r^2}{l}\frac{\partial H_1}{\partial r} + \frac{2r}{l}H_1\right)\right]\end{aligned} \quad (4.46)$$

and the complete integrand reads

$$\frac{1}{\Omega}\left\{H_0, \frac{H_1}{\Omega}\right\} = -u^r\frac{r^3}{l^2}\left[r\frac{\partial H_0}{\partial r}\frac{g^{(1)}_{rr}}{g^{(0)}_{rr}} + 2H_1 + r\frac{\partial H_1}{\partial r}\right]. \quad (4.47)$$

Inserting one of the above derived relativistic homoclinc orbits and integrating along it leads to the relativistic Melnikov function

$$M(\vartheta_0) = \int_{-\infty}^{\infty}\left\{(-u^r)\frac{r^3}{l^2}\left[r\frac{\partial H_0}{\partial r}\frac{g^{(1)}_{rr}}{g^{(0)}_{rr}} + 2H_1 + r\frac{\partial H_1}{\partial r}\right]\right\}(r(\vartheta), u^r(\vartheta), \vartheta + \vartheta_0)\mathrm{d}\vartheta. \quad (4.48)$$

Dependencies of the integrand are written behind the curly bracket while the dependence on the fixed parameters l and l_z is not explicitly shown. As in the previous case the homoclinic orbit is expressed using the variable $u(\vartheta)$, where

$$r(\vartheta) = \frac{1}{u(\vartheta)}, \qquad u^r(\vartheta) = \frac{\mathrm{d}r}{\mathrm{d}\tau}(\vartheta) = -l\frac{\mathrm{d}u(\vartheta)}{\mathrm{d}\vartheta}, \qquad p_r = m_0 g^{(0)}_{rr} u^r.$$

The Melnikov integrals (4.44) and (4.48) may now be evaluated numerically and we shall see that they indeed have simple zero points.

4.6 Results and their numerical verification

We can now plot the Melnikov functions and investigate their dependence on parameters. I will present here the results for the pseudo-Newtonian superposition of the Schwarzschild black hole and the inverted Morgan-Morgan disc or the Bach-Weyl ring, and for the extreme Reissner-Nordström black hole surrounded by the Majumdar-Papapetrou ring.

The Melnikov functions will be plotted on the interval $(0, \pi)$ as they are periodic with period π. Although the functions are rather complicated and cannot be expressed in a closed form, their plots are surprisingly simple: they mostly exhibit a very sine-like behaviour as can be seen in figure 4.8a, while the shape shown in figure 4.8b is much less frequent.

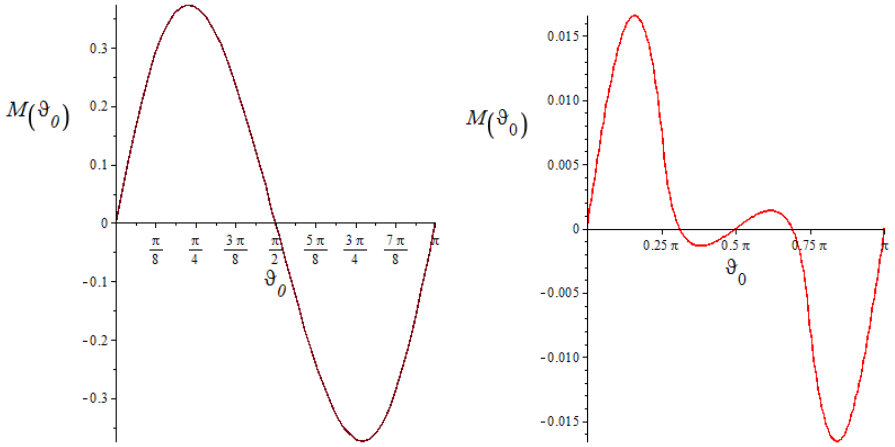

(a) (b)

Figure 4.8: (a) Extreme RN black hole with the MP ring ($b = 15M, l = 3M, l_z = 0$). (b) Pseudo-Newtonian Schwarzschild black hole with the inverted MM disc ($b = 6M, l = 2.5M, l_z = 1M$).

The Melnikov function $M(\vartheta_0)$ depends on three fixed parameters which can scale with the black hole mass M. Apart from the ring/disc radius b being the obvious constant of the system, we have the z-component of the angular momentum l_z and the total angular momentum l (we again work with normalized quantities). The angular momentum l selects one particular homoclinic orbit, but it is not an integral of motion of the complete system. (The angular momentum l can be exchanged for the energy e which also uniquely determines a homoclinic orbit, but for now we will use l.)

The first parameter we will investigate is l_z. Changing this quantity while having b and l fixed has the same effect on the Melnikov function, no matter which of our gravitational sources we consider. Since l_z is just a component of the angular momentum vector with magnitude l we have $l_z \in \langle 0, l \rangle$ (we use only positive l_z). If l_z approaches l, Melnikov-function amplitude decreases before finally becoming identically zero,

$$\lim_{l_z \to l} M(\vartheta_0) = 0.$$

Such a result is not unexpected. For $l_z = l$ the motion is confined to the equatorial plane which is the plane of the disc/ring. From the point of view of this equatorial plane, spherical symmetry is not broken by perturbation and the complete system is independent of ϑ, so for a small perturbation the degenerate homoclinic orbit is preserved (W^s and W^u coincide along it).

The dependence of Melnikov functions on l_z is plotted in figure 4.9. For the relativistic extreme RN black hole with MP ring the results are practically the same.

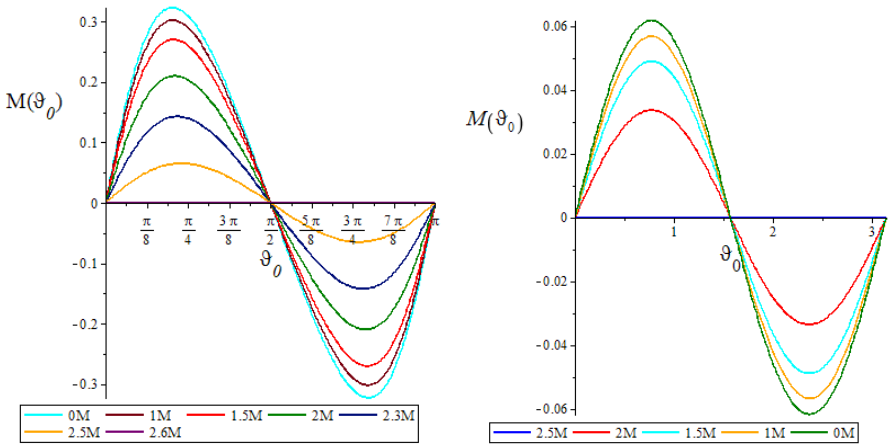

(a) (b)

Figure 4.9: Dependence of $M(\vartheta_0)$ on l_z for pseudo-Newtonian Schwarzschild black hole with the inverted MM disc ($b = 20M, l = 2.6M$) (a) and with the BW ring with the ($b = 20M, l = 2.5M$) (b).

We can conclude that $M(\vartheta_0)$ has maximum amplitude for $l_z = 0$, which however does not have much importance since the only significant result is the existence of zero points.

Another parameter we can change is the ring/disc radius b. With growing radius the amplitude of $M(\vartheta_0)$ drops down before finally becoming zero. This is a consequence of the fact that the perturbation H_1 gradually vanishes,

$$\lim_{b \to \infty} H_1 = 0 \Rightarrow \lim_{b \to \infty} M(\vartheta_0) = 0.$$

This result clearly stems from the fact that a ring/disc cannot affect the motion around a black hole from which it is infinitely far away. Setting $b = \infty$ is thus equivalent to an unperturbed system and therefore the degenerate homoclinic orbit remains unchanged, which leads to $M(\vartheta_0) = 0$.

The opposite limit is $b \to 0$. To evaluate the Melnikov function for $b = 0$ we first need to find how our perturbations look in this case. The simplest case is the Majumdar-Papapetrou ring whose lapse function N (2.17) reduces to that of the extreme Reissner-Nordström black hole (2.14). So in total we are left with a RN black hole of double mass at the centre which again leads to $\lim_{b\to 0} M(\vartheta_0) = 0$. The first metric functions $\nu(\rho, z)$ of the inverted MM disc and of the BW ring have the same limit,

$$\lim_{b\to 0} \nu(\rho, z)_{BW/MM} = -\frac{m}{\sqrt{\rho^2 + z^2}}.$$

This corresponds to a point particle located at the origin (its relativistic counterpart would be the Curzon-Chazy metric). So one would expect preservation of the spherical symmetry and thus vanishing of the Melnikov function. This actually happens, but only if we perform the transformation between cylindrical and spherical coordinates using the Euclidean relations

$$\rho = r \sin\theta \qquad z = r \cos\theta.$$

If we use the relativistic relations (2.6) instead, we get a non-zero $M(\vartheta_0)$ with its typical sine-like behaviour. So we see that choosing the right coordinate transformation can be rather tricky. In this particular situation we interpret the sources in a Newtonian fashion which means that we assume the space to be flat and so the Euclidean transformation relation turns out to be more adequate.

The dependence of the Melnikov function on radius b can be seen in figure 4.10.

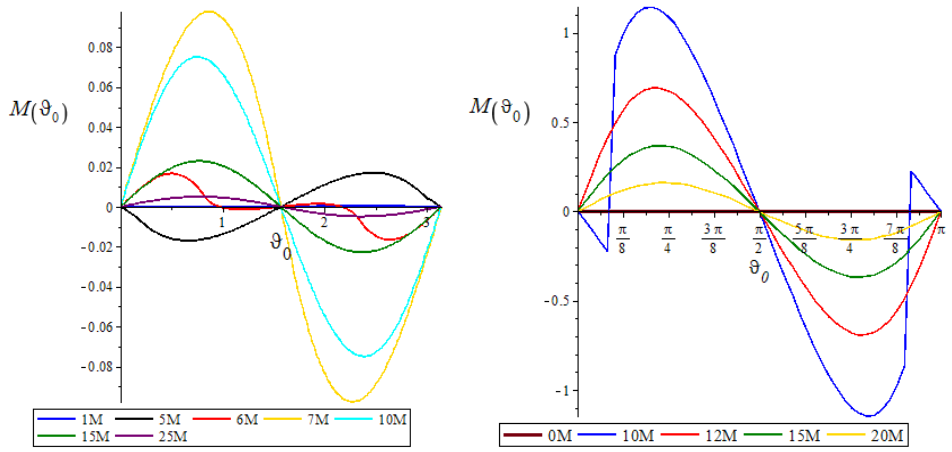

(a) (b)

Figure 4.10: Radius dependence of $M(\vartheta_0)$ for pseudo-Newtonian Schwarzschild black hole with the inverted MM disc ($l = 2.5M, l_z = 1M$) (a), and for the extreme RN black hole with the MP ring ($l = 3M, l_z = 1M$) (b).

Before continuing the study of parameter dependences, we should address a problem which occurs when one changes the radius of the ring/disc. While integrating the expression given by Poisson brackets, it may happen that the integration path (homoclinic orbit) crosses the equatorial plane exactly where the ring or disc is located, which is however a singular place of our perturbations

(and their derivatives). The Melnikov function $M(\vartheta_0)$ thus becomes discontinuous for some values of ϑ_0, actually the method may potentially break down in such

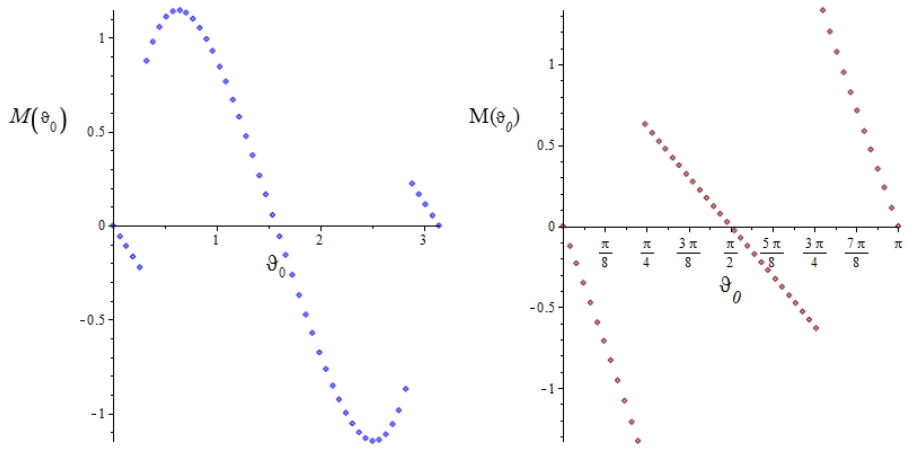

(a) (b)

Figure 4.11: Two graphs of different $M(\vartheta_0)$ with discontinuities, obtained for corresponding the extreme RN black hole with the MP ring. The jumps are commented in the main text.

a case. However, the function still has zero points and in their neighbourhood it is continuous (figure 4.11), so this could lead to the existence of transverse homoclinic points anyway. This point needs further study for sure.

The last parameter we have not discussed yet is the total angular momentum l (which can be replaced by either J_ϑ or the energy e). This dependence is actually the least interesting since the amplitude of $M(\vartheta_0)$ simply increases with l (figure 4.12) ranging within its respective interval (see below).

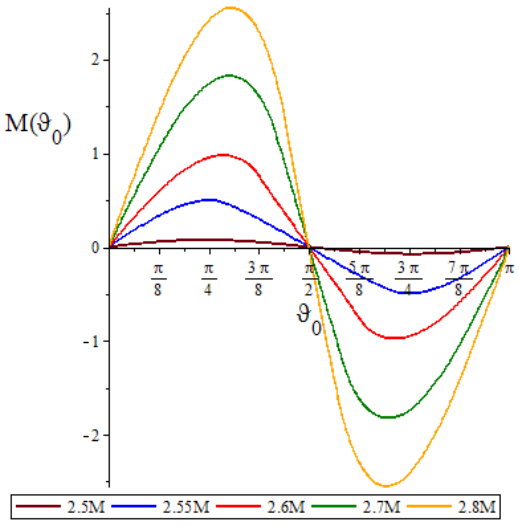

Figure 4.12: The dependence of $M(\vartheta_0)$ on the total angular momentum l for pseudo-Newtonian Schwarzschild black hole with the inverted MM disc ($b = 10M, l_z = 1M$)

As we have seen, for all the values of the parameters (with some special exceptions like $l_z = l$) the Melnikov function $M(\vartheta_0)$ has simple zero points which proves

the existence of transverse homoclinic orbits and therefore chaotic behaviour in their vicinity. We can guess that the results would be the same for the relativistic superposition.

Now an obvious question arises: Does the existence of zero points of $M(\vartheta_0)$ lead to the conclusion that even for a very small perturbation the dynamics turns chaotic for every value of the parameters? The answer is obviously no, as the degenerate homoclinic orbit (which splits under perturbation) exists only for some values of the parameters and that is what we will discuss now.

If we take a look at the relations for the (coordinate) radius $r_{\rm hyp}$ of the unstable circular orbit (relations (4.30), (4.35) and (4.38)), we can notice that it contains square root of some argument which is positive only for some range of l. This allows us to determine the minimal value of the angular momentum ($l_{\rm min}$) for which there exists the unstable circular orbit (we express l in units of M thus eliminating the dependence on the black-hole mass).

For the (degenerate) homoclinic orbit to exist, an additional condition must be fulfilled: there has to be a turning point which corresponds to the maximal distance $r_{\rm max}$. For our effective potential this means

$$V_{\rm eff}(r_{\rm hyp}) \leq \lim_{r\to\infty} V_{\rm eff}(r).$$

The equality in this equation corresponds to the maximal value $l_{\rm max}$, for $l > l_{\rm max}$ the unstable circular orbit still exists but there is no homoclinic orbit connected to it so, to summarize, the homoclinic orbit exists for $l \in (l_{\rm min}, l_{\rm max}\rangle$. The conditions on l can be converted to the conditions on e and l_z which in contrast to l are integrals of motion of the perturbed system. The energy of the homoclinic orbit is uniquely given by the angular momentum, $e = e(l)$, so the energy condition can be written as $e \in (e_{\rm min}, e_{\rm max}\rangle$ with $e_{\rm min} = e(l_{\rm min})$ and $e_{\rm max} = e(l_{\rm max})$. It is easy to deduce that $e_{\rm max} = V_{\rm eff}(r \to \infty)$.

By the particle energy e, the geodesics in the unperturbed system can be divided into three groups independently of their angular momentum:

1. $e < e_{\rm min}$: Geodesics which always end in the black hole and cannot reach infinity (or come from there).

2. $e \in (e_{\rm min}, e_{\rm max}\rangle$: Bound orbits and also geodesics that end in the black hole. These also cannot exist at asymptotic radii.

3. $e > e_{\rm max}$: Geodesics that can arrive to or from infinite r. These geodesic may end in the black hole or be reflected by the potential barrier.

We can expect that the same behaviour occurs in the perturbed system provided that the perturbation is small enough. As expected, only the second of the cases above leads to chaotic dynamics since only in that case there are bound orbits separated from the infalling orbits by a separatrix (homoclinic orbit) that splits into the asymptotic manifolds after perturbation. The three different situations are depicted in figure 4.13.

The condition for the other integral of motion l_z is natural. As $l_z \leq l$, the z-component of angular momentum must satisfy $l_z \leq l_{\rm max}$. If this condition does not hold true, then $l > l_z > l_{\rm max}$, which is in contradiction with $l \in (l_{\rm min}, l_{\rm max}\rangle$. On the other hand if $l_z < l_{\rm min}$, then the other components of angular momentum

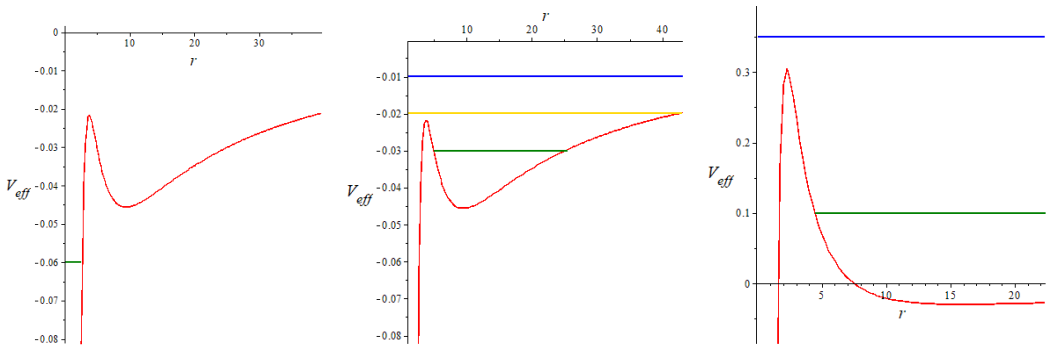

(a) (b) (c)

Figure 4.13: Pseudo-Newtonian effective potential of the Schwarzschild black hole with energies satisfying $e < e_{\min}$ (a), $e \in (e_{\min}, e_{\max}\rangle$ (b), $e > e_{\max}$(c).

can still add up to l belonging to the required interval (as we have seen above, it is in fact necessary that $l_z \neq l$). The intervals of l and e for which there exists a homoclinic orbit can be seen in table 1.

Table 1: conditions for existence of homoclinic orbits			
potential	Nowak-Wagoner	Schwarzschild	extreme RN black hole
interval of l	$(\sqrt{6}M, \sqrt{8\sqrt{3}-6}M)$	$(2\sqrt{3}M, 4M)$	$(2\sqrt{3}M, \frac{1}{2}\sqrt{22+10\sqrt{5}}M)$
interval of e	$(-\frac{1}{18}, 0)$	$(\frac{2}{3}\sqrt{2}, 1)$	$(\frac{3}{8}\sqrt{6}, 1)$

Therefore the final conclusion of the Melnikov method for our system of a perturbed black hole reads:

On the hypersurface given by $e \in (e_{\min}, e_{\max}\rangle$ and $l_z \in \langle 0, l_{\max})$ there exist transverse homoclinic orbits in whose neighbourhood the system exhibits a chaotic behaviour.

The final part of this chapter will be dedicated to the numerical verification of the results obtained by this analytic method. For that purpose we shall again use the code by M. Žáček.

We will test the method on the superposition of an extreme RN black hole with the MP ring, as it is the only fully relativistic system for which we have computed the Melnikov function. To find some chaotic orbits, we need to properly choose values of the integrals of motion. We fix the values as $e = 0.942809$ and $l_z = 1M$. One can check that these values indeed fall within the intervals given in table 1.

We start with the unperturbed system containing only the extreme Reissner-Nordström black hole. We choose an orbit close to the separatrix whose Poincaré section can be seen in figure 4.14. It is a smooth curve as we would expect for a regular orbit. In the unperturbed system the bound orbits are strictly separated from the infalling orbits by the separatrix. What does happen if we add a perturbation in the form of the MP ring? We set a small perturbation mass $m = 0.01M$ and again check the orbits close to the original separatrix, especially focusing on the points close to the unstable periodic orbit. The resulting Poincaré section of one such orbit is plotted in figure 4.15, with the neighbourhood of the unstable fixed point displayed in more detail in part (b) of 4.15 and also in figure 4.16 where three close orbits are shown.

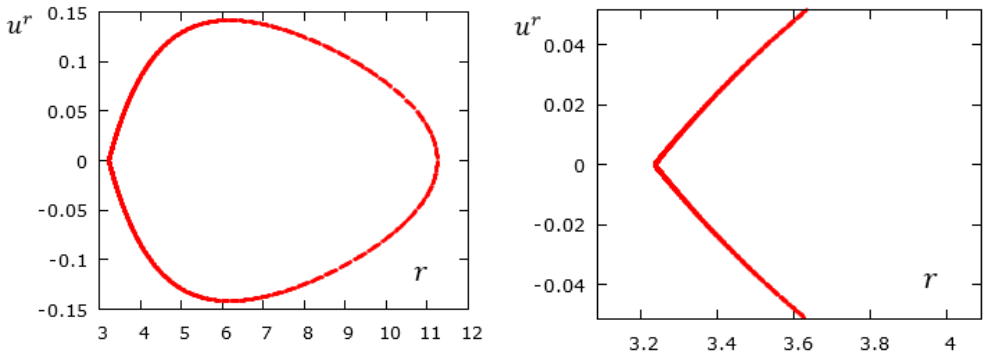

(a) (b)

Figure 4.14: Poincaré section of an orbit around an unperturbed extreme RN black hole close to the separatrix (a) and its detail close to the fixed point (b) (with $e = 0.942809$, $l_z = 1M$).

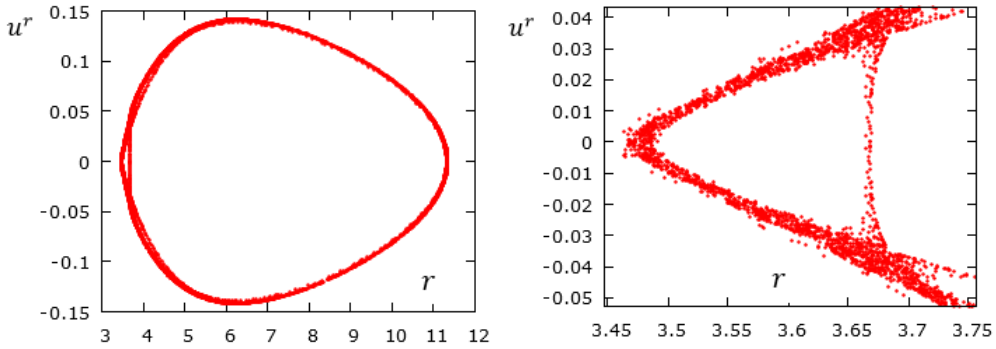

(a) (b)

Figure 4.15: Poincaré section of an orbit ($e = 0.942809$, $l_z = 1M$) around the extreme RN black hole perturbed by the MP ring ($m = 0.01M$) close to the original separatrix (a) and in detail (b).

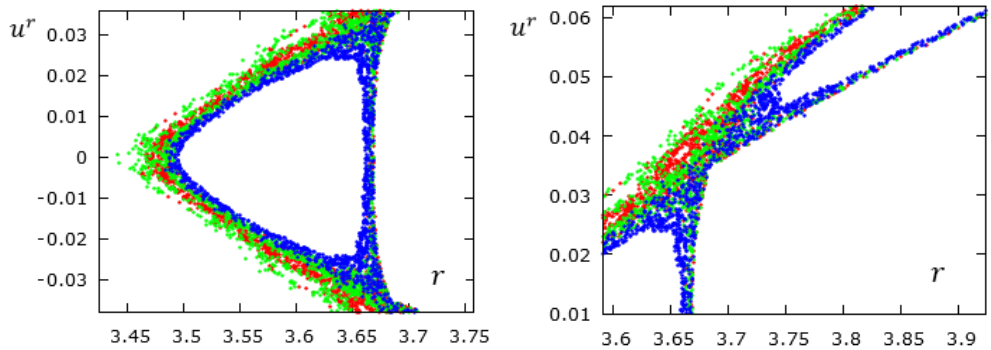

(a) (b)

Figure 4.16: A detailed look at the dynamics of 3 different orbits ($e = 0.942809$, $l_z = 1M$) close to the unstable periodic orbit in the system of the extreme RN black hole perturbed by the MP ring with $m = 0.01M$.

It is evident that the geodesics densely fill a certain area in the Poincaré section confirming their chaotic nature. But for our answer to be complete we have to find how far from the unperturbed separatrix the chaotic behaviour persists.

In figure 4.17 we can see that if we do not focus on the neighbourhood of the separatrix, we do not notice any sign of chaotic dynamics. In fact the whole inner part of the Poincaré section is filled with smooth curves of regular bound orbits. The blank part of the allowed region in 4.17 corresponds to the orbits plunging into the black hole. So between the bound-orbits region and the infalling orbits there is a thin chaotic layer (figures 4.15 and 4.16) at the place where the unperturbed separatrix was located.

A very similar result was obtained by Aslanov [2015] who studied a very different system (tow of space debris by a tether) and also numerically verified his results obtained by the Melnikov method.

Thus we have shown that the only chaotic behaviour in the system of a black hole and a small perturbation has homoclinic origin and that the chaotic regions are concentrated in a small part of some hypersurfaces in the phase space. Otherwise the dynamics in this nearly integrable system remains regular.

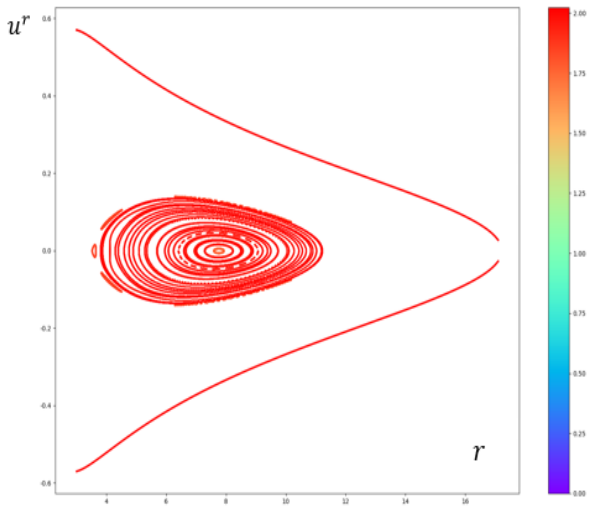

Figure 4.17: Bound orbits in the system of an extreme RN black hole perturbed by the MP ring with parameters $m = 0.01M$, $e = 0.942809$, $l_z = 1M$.

Before the end of this chapter let me add some remarks concerning the Melnikov method. The standard Melnikov method has numerous generalizations, for example to the case when neither the unperturbed system nor the perturbation are Hamiltonian in nature. This allows applications to dissipative systems (drag forces, friction,...); some examples are given in Wiggins [2000]. There is also a generalization where the integral is taken along a heteroclinic orbit. Most importantly, there exists a generalization to higher degree-of-freedom systems (see Gruendler [1985]) which are much more complicated. They for example require a complete solution of the variational equation of the unperturbed system along the homoclinic orbit, which is mostly impossible to find analytically. Fortunately, I have managed to avoid any higher-dimensional generalization thanks to the canonical transformation.

Concerning the application of this method in general relativity, there have

been at least three articles involving the perturbation of the Schwarzschild black hole. The first was the relativistic version of the classical Hill problem Moecker [1992]. The article by Santoprete and Cicogna [2002] used uniform electric and magnetic fields as perturbations. In these two articles the authors used different modification of the one-degree-of-freedom Melnikov method.Finally in the article by Bombelli and Calzetta [1992] it is the gravitational waves what plays the role of a perturbation, and the classical formulation of the method is used. The perturbed motion in this case remains planar, so the authors did not need to deal with the problem of multiple degrees of freedom.

Conclusion

Motivated by theoretical interest as well as accreting black holes in astrophysics, we have studied time-like geodesic dynamics in the space-time of a static black hole perturbed by a ring or a disc using two analytical methods and subsequently confronted their results with numerical simulations.

The first method, the geometric criterion which should indicate the tendency to chaos on the basis of properties of the Riemann tensor, turned out to play the role of a necessary condition for the appearance of chaos in the system of a black hole encircled by a ring. For a black hole surrounded by a disc, the criterion is neither suffcient nor necessary. We have conjectured that such a failure may arise due to the particles' repeated crossing of the (infinitely thin, thus non-smooth) disc which may possibly lead to chaos even without any contribution from a "diverging" region. Replacing the quantifiers based on the geometric criterion by the number of disc crossings really leads to better results, but there are some situations when this estimate also fails. Therefore, although there is definitely a connection between geodesic dynamics and the configuration-space geometry, the curvature criterion tested in this thesis is not always a reliable indicator of chaos, which is also the conclusion that most authors support.

The other method considered was that by Melnikov. This concentrates on the homoclinic chaos caused by break-up of a homoclinic orbit due to the perturbation. In order for the Melnikov method to be applicable to our systems, we have made a canonical transformation of the respective hamiltonians. For all our systems the Melnikov function was found to have simple zeros which is the proof that the transverse homoclinic orbits exist in the phase space, which in turn leads to the creation of a chaotic layer in the neighbourhood of the location where there originally (before perturbation) was a separatrix. In agreement with the Melnikov theory, for a small perturbation the chaotic orbits only occur in a small part of some hypersurfaces in the phase space given by integrals of motion for which the degenerate homoclinic orbit (separatrix) exists. The results of the Melnikov method were verified numerically in the electro-vacuum Majumdar-Papapetrou space-time generated by an extreme Reissner-Nordström black hole encircled by an extremally charged ring. It can be expected that for superpositions with the Schwarzschild black hole the results would be similar.

In my opinion the most important contribution of the thesis is the usage of canonical transformation which permitted to rewrite the hamiltonian to the form required by the Melnikov method. This approach could actually be applied to a central field with any axially symmetric perturbation, and it is quite simple in comparison with the generalizations of the method to more degrees of freedom used by other authors.

Bibliography

Y. Asano, H. Kyono, and K. Yoshida. Melnikov's method in String Theory. *Journal of High Energy Physics*, 2016, 2016.

V. Aslanov. Chaos Behaviour of Space Debris During Tethered Tow. *Journal of Guidance, Control and Dynamics*, 39(10):2399–2405, 2015.

J. Banks, J. Brooks, G. Cairns, G. Davis, and P. Stacey. On Devaney's definition of chaos. *The American Mathematical Monthly*, 99(4):332–334, 1992.

L. Bombelli and E. Calzetta. Chaos around a black hole. *Classical and Quantum Gravity*, 9:2573–2599, 1992.

P. M. Cincotta and C. Simó. Simple tools to study global dynamics in non-axisymmetric galactic potentials-I. *Astronomy, Astrophzsics supplement series*, 147:205–228, 2000.

I. Coppo and V. Rougier. The new chaotic pendulum, 2012. URL `http://physique.unice.fr/sem6/2011-2012/PagesWeb/PT/Pendule/En/more3.html`.

R. L. Devaney. *An introduction to chaotic dynamical systems*. Second edition. Addison-Wesley Publishing Company, 1989. ISBN 0-201-13046-7.

J. B. Griffiths and J. Podolský. *Exact Space-Times in Einstein's General Relativity*. Second Edition. Cambridge University Press, Cambridge, 2009. ISBN 978-0-521-88927-8.

J. Gruendler. The existence of homoclinic orbits and the method of Melnikov for systems in R^n. *SIAM Journal on Mathematical Analysis*, 16(5):907–931, 1985.

P. J. Holmes and J. E. Marsden. Horseshoes and Arnold diffusion for Hamiltonian Systems on Lie groups. *Indiana University Mathematics Journal*, 32:273–309, 1983.

A. J. Lichtenberg and M. A. Lieberman. *Regular and Chaotic Dynamics*. Second Edition. Springer-Verlag New York, New York, 1983,1992. ISBN 3-540-97745-7.

N. P. Maffione, C. M. Giordano, and P. M. Cincotta. Testing a Fast Dynamical Indicator: The MEGNO. *International Journal of Non-Linear Mechanics*, 46: 23–34, 2011.

D. Merritt. Elliptical galaxy dynamics, 1999. URL `https://ned.ipac.caltech.edu/level5/March01/Merritt2/Merritt2.html`.

R. Moecker. A nonintegrable model in General Relativity. *Communications in Mathematical Physics*, 150:415–430, 1992.

K. Ramasubramanian and M. S. Sriram. Global geometric indicator and Lyapunov exponents in Hamiltonian systems. *Physical review E*, 64:046207, 2001.

A. Saa. On the viability of local criteria of chaos. *Annals of Physics*, 314:508–516, 2004.

E. Sander and J. A. Yorke. Chaos and its Manifestations, 2015. URL `https://sinews.siam.org/Details-Page/chaos-and-its-manifestations`.

M. Santoprete and G. Cicogna. Chaos in Black Holes Surrounded by Electromagnetic Fields. *General relativity and gravitation*, 34(7):1107–1119, 2002.

O. Semerák. Static axisymmetric rings in general relativity: How diverse they are. *Physical Review*, 94:104021, 2016.

O. Semerák and P. Suková. Free motion around black holes with discs or rings: between integrability and chaos - I. *Monthly Notices of the Royal Astronomical Society*, 404:545–574, 2010.

Y. Sota, S. Suzuki, and K. Maeda. Chaos in static axisymmetric spacetimes: I. Vacuum case. *Classical and Quantum Gravity*, 13:1241–1260, 1996.

P. Stránský and P. Cejnar. Study of curvature-based criterion in Hamiltonian systems with two degrees of freedom. *Journal of Physics A: Mathematical and Theoretical*, 48(12):125102, 2015.

M. Szydłowski. Curvature of gravitationally bound mechanical systems. *Journal of Mathematical Physics*, 35(4):1850–1880, 1994.

S. Wiggins. *Introduction to Applied Nonlinear Dynamical Systems and Chaos*. Second Edition. Springer-Verlag New York, Bristol, 2000. ISBN 0-387-00177-8.

V. Witzany, O. Semerák, and P. Suková. Free motion around black holes with discs or rings: between integrability and chaos - IV. *Monthly Notices of the Royal Astronomical Society*, 451:1770–1794, 2015.